AD A126214

|	
Technical Report	620
	W. Rotman
EHF Dielectric Lens Antenna for Satellite Communication Systems	
	3 January 1983

Lincoln Laboratory

MASSACHUSETTS INSTITUTE OF TECHNOLOGY

LEXINGTON, MASSACHUSETTS

DTIC FILE COPY

DTIC

MAR 3 1 1983

A

83 03 30 051

This technical report has been reviewed and is approved for publication.

FOR THE COMMANDER
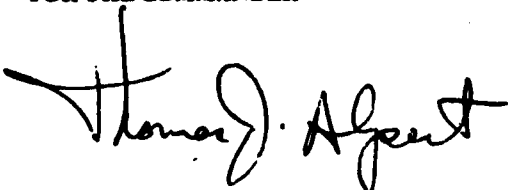
Thomas J. Alpert, Major, USAF
Chief, ESD Lincoln Laboratory Project Office

MASSACHUSETTS INSTITUTE OF TECHNOLOGY

LINCOLN LABORATORY

EHF DIELECTRIC LENS ANTENNA FOR SATELLITE COMMUNICATION SYSTEMS

W. ROTMAN

Group 61

TECHNICAL REPORT 620

3 JANUARY 1983

LEXINGTON   MASSACHUSETTS

ABSTRACT

Dielectric lens antennas are applicable to the design of multiple-beam antenna (MBA) systems on EHF communication satellites. Advantages include excellent wide angle scanning properties and elimination of feed blockage. This report describes an experimental 90λ dia. zoned dielectric lens, operating at 44 GHz, which was fabricated and tested in order to estimate the performance of a dielectric lens MBA. Measurements showed that the lens generated a beam with a half-power beamwidth (HPBW) of $0.7°$ which could be steered over a total scan angle of $18°$ (corresponding to the earth's field-of-view from a geosynchronous satellite) with a scanning loss of less than 1 dB and a gain in excess of 47 dBi measured at the sub-satellite point over a 5% bandwidth. A theoretical analysis of the radiation characteristics of the lens antenna, using ray tracing and geometric optics techniques, gave excellent agreement with the measurements. Simplified design equations were developed to facilitate evaluation and development of lens antenna systems of this type.

iii

CONTENTS

ILLUSTRATIONS

ILLUSTRATIONS (cont'd)

TABLES

I. INTRODUCTION

Multiple-beam antennas (MBAs) are currently being considered for use on military satellites operating at EHF in order to obtain high gain and spatial resolution[1,2]. For this service, these antennas should be capable of directing either spot beams or clusters of beams from a satellite in synchronous orbit to any point on the earth's surface. The principal antenna candidates for this application use either lenses or offset reflectors. The lens antenna has certain advantages as a multiple beam antenna (MBA), including elimination of feed blockage and excellent wide angle scanning properties. Although it is generally too heavy or complex at the lower microwave frequencies when beamwidths of less than one degree are required, at millimeter wavelengths a zoned dielectric lens with a diameter of two feet weighs on the order of ten pounds. This size antenna can provide a directive gain of 48 dBi at 44 GHz. Furthermore, this gain does not decrease significantly with scan angle.

A basic application for the lens MBA is depicted in Figure 1 which shows an EHF MBA on a geosynchronous satellite. The switching network within the antenna selects one or more elements of the feed array to illuminate the lens and form a beam directed towards the desired coverage area on the earth's surface.

The principal topic of this report is the design and test of a dielectric lens with wide-angle scanning capabilities for this application. The design of the beam-forming network and feed arrays for the lens antenna will not be considered here. Similarly, the feed horns which are used to illuminate the

1
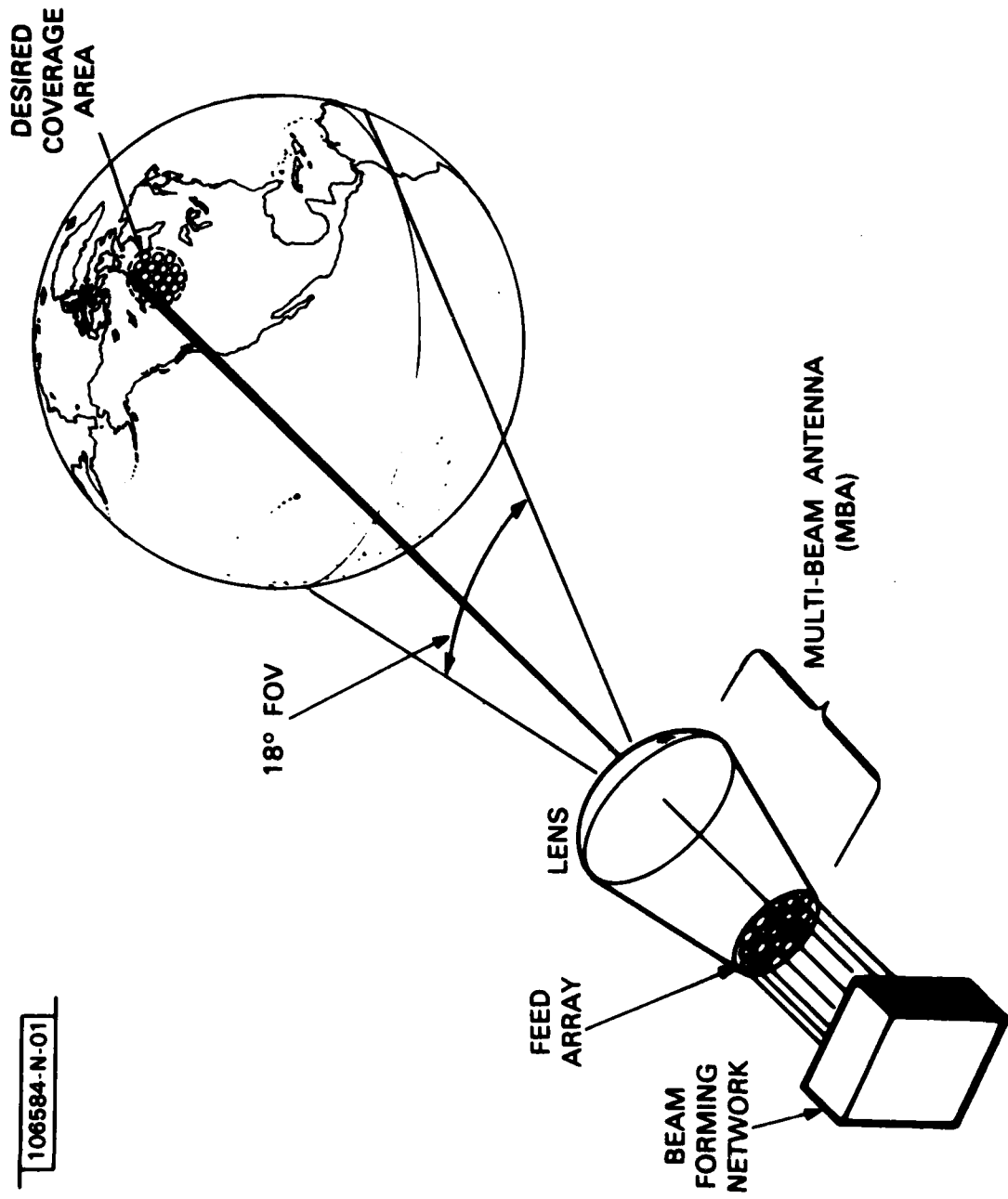
Fig. 1. Lens antenna system for satellite communications.

DESIRED COVERAGE AREA

18° FOV

LENS

MULTI-BEAM ANTENNA (MBA)

FEED ARRAY

BEAM FORMING NETWORK

106584-N-01

2

lens are analyzed only to the extent to which this serves the evaluation of the lens performance.

A major problem in the design of this multiple-beam lens antenna is the requirement to direct a beam with a fractional degree beamwidth from a satellite over the entire earth's field-of-view (?) of 18° total scan angle without incurring excessive reduction of gain. 's decrease in directivity with scan angle will be shown to be related to th :f-axis aberrations of the lens, which are minimal for an idealized spherica ¸s of zero thickness with its focal point at its center of curvature. Although this ideal cannot be achieved in practice, it can be approximated by zoning, or stepping the thickness of the lens. This zoning also has the beneficial effect of reducing the weight of the lens; however, these benefits are partially offset by an increase in frequency sensitivity. Partial zoning offers a reasonable compromise for many applications between off-axis performance, bandwidth, and weight considerations.

The decrease in gain of the lens, caused by variations in frequency from the design value and by scanning along an optimum focal path, can be estimated from the simple thin lens equations, presented in Section III, which are appropriate for zoned lenses with spherical outer faces. Figure 2 shows this loss $L(\alpha)$ as a function of scan angle α for 90λ (diameter) lenses with seven zones and with focal length to diameter (F/D) ratios of either 1.0 (dashed lines) or 1.5 (solid lines). The two curves for each F/D ratio represent the losses at the center, or design frequency ($f = f_0$; $\Delta f = 0$), and at the band edges ($\Delta f/f_0 = \pm 2.5\%$), respectively. (These curves are obtained as special

3
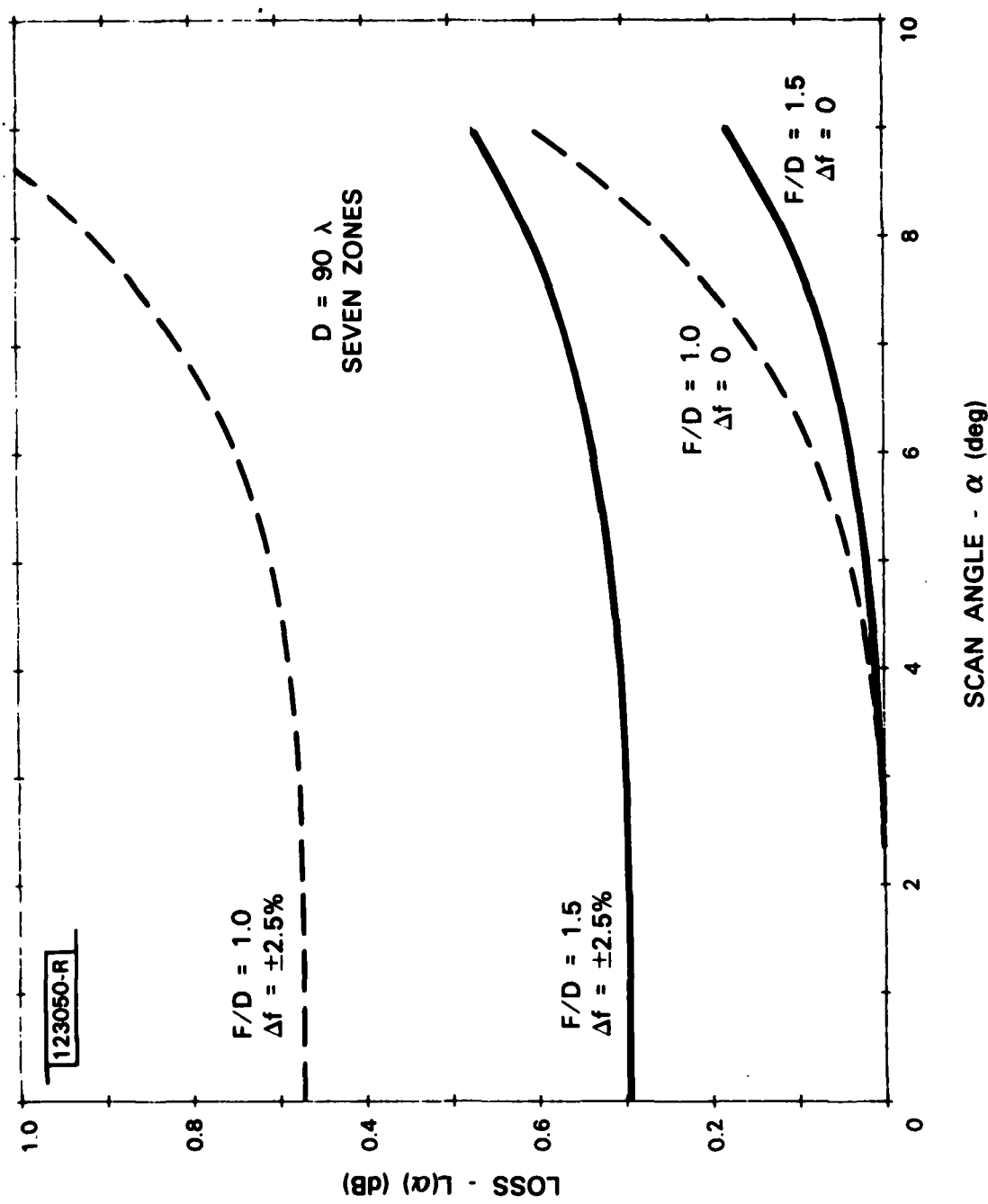
Fig. 2. Loss of directive gain with scan angle for coma-corrected lens.

123050-R

D = 90 λ
SEVEN ZONES

F/D = 1.0
Δf = ±2.5%

F/D = 1.5
Δf = ±2.5%

F/D = 1.0
Δf = 0

F/D = 1.5
Δf = 0

SCAN ANGLE - α (deg)

LOSS - L(α) (dB)

cases of the general scanning loss curves of Fig. 21). These estimates predict that for our experimental lens (90λ, F/D = 1.5, 7 zones), the scanning losses over the earth's FOV (± 9°) should be less than 0.2 dB at the design frequency and 0.5 dB at the band edges. The excellent scanning characteristics of the lens, which these values predict, have been verified generally by the more accurate ray trace analyses and antenna measurements which are described in this report.

A qualitative comparison of the scanning performance of lens antennas with various types of reflectors is instructive in evaluating potential system applications. Prior studies[3,4] have shown that the loss in gain with scan angle of symmetrical, coma-corrected reflectors and of thin lenses with the same F/D ratios are identical. However, since the feed in a reflector usually is offset from its axis of symmetry in order to prevent obscuration of the aperture, scanning must be essentially one-sided in the offset plane. Furthermore, the simple parabolic reflector is not coma-corrected. (Although this could be accomplished by stepping its surface, the resultant reflector would then be frequency-sensitive, similar to the lens.) The zoned dielectric lens would, therefore, be expected to have superior scan characteristics over any prime-focus symmetrical reflector system of the same F/D ratio since offsetting is not necessary and the lens is essentially coma-corrected.

Some improvement may be achieved in the beam steering characteristics for an asymmetrical offset-fed reflector so that it has same phase errors[5] (third order) as a symmetrical reflector for equal displacement of the feed laterally from the prime focus. Although this change avoids the offsetting

5

loss which is inherent in the symmetrical systems, the reflector scan still must be single-sided and, therefore, inferior to lens scanning. The situation is not so clear for offset Cassegrain reflector systems, however. In this case, the scanning performance can be evaluated from the equivalent parabola concept in which the equivalent focal length is increased over the physical focal length by the magnification factor of the antenna system. The equivalent F/D ratio may, therefore, be several times that of a lens with the same physical dimensions with a corresponding improvement in scan capability. Since this advantage will be partially nullified by the one-sided scan requirement of the offset reflector, the lens and Cassegrain reflector are likely to have comparable beam steering properties although an exact evaluation can probably only be made on a case-by-case basis.

6

II. SELECTION OF LENS PARAMETERS

Although the weight of the lens is a major factor affecting its design for satellite applications, light weight artificial dielectric and constrained lenses were excluded from consideration because of their complexity and difficulty of fabrication at EHF frequencies. An unzoned dielectric lens of 90λ diameter (the design dimension) is relatively heavy at Q band (44 GHz), ranging up to almost 70 pounds for a solid lens (polyethylene) with an F/D of 1.0. This weight can be drastically reduced through zoning and increasing the F/D ratio. (This also has the commensurate effect of reducing the scanning losses, as previously mentioned.)

The zoning consists of stepping the rear surface of the lens whenever its thickness exceeds a differential path length of one optical wavelength difference plus a minimum value T_0. A fully zoned lens is obviously the minimum weight solution. However, its bandwidth is restricted, as expressed by the relation[6]:

$$\text{Bandwidth} = \frac{25}{N} \% \qquad (1)$$

where N is the number of steps. (Equation 1 assumes a maximum phase variation at the edge of the lens of $\lambda/8$, corresponding to a zoning phase loss[7] of 0.5 dB. Additional losses might also occur because of scattering and diffraction by the zoning steps.) A dielectric lens antenna with a bandwidth of 5% would, therefore, be nominally limited to five steps (N = 5) whereas a fully zoned 90λ lens with F/D of 1.5 requires eight steps. As a compromise,

7

six steps were used in the experimental model, accepting the increased scan loss at the frequency band limits.

The design of the lens (Figures 3 and 4) follows exactly the detailed procedure given in reference 8, except that the lens is partially, rather than completely, zoned. Detailed dimensions of this lens, including its scaled cross-section, are presented in Appendix A. Its outer (front) surface is spherical, with the center of curvature at the focal point. The inner (rear) surface is determined by equating the optical path length of a ray from the focal point through the lens to that of the central ray (Figure 5) (stepping the lens thickness whenever it exceeds a differential wavelength). For machining, the central and first outer zones for the inner surface of the lens are represented by a fourth degree polynomial; the outer five zones are approximated by straight line segments, determined by the points of discontinuity and corners on the contour. These approximations specify the inner contour of the lens to within two mils of the theoretical surface. The lens was machined on a numerically controlled lathe in accordance with these specifications.
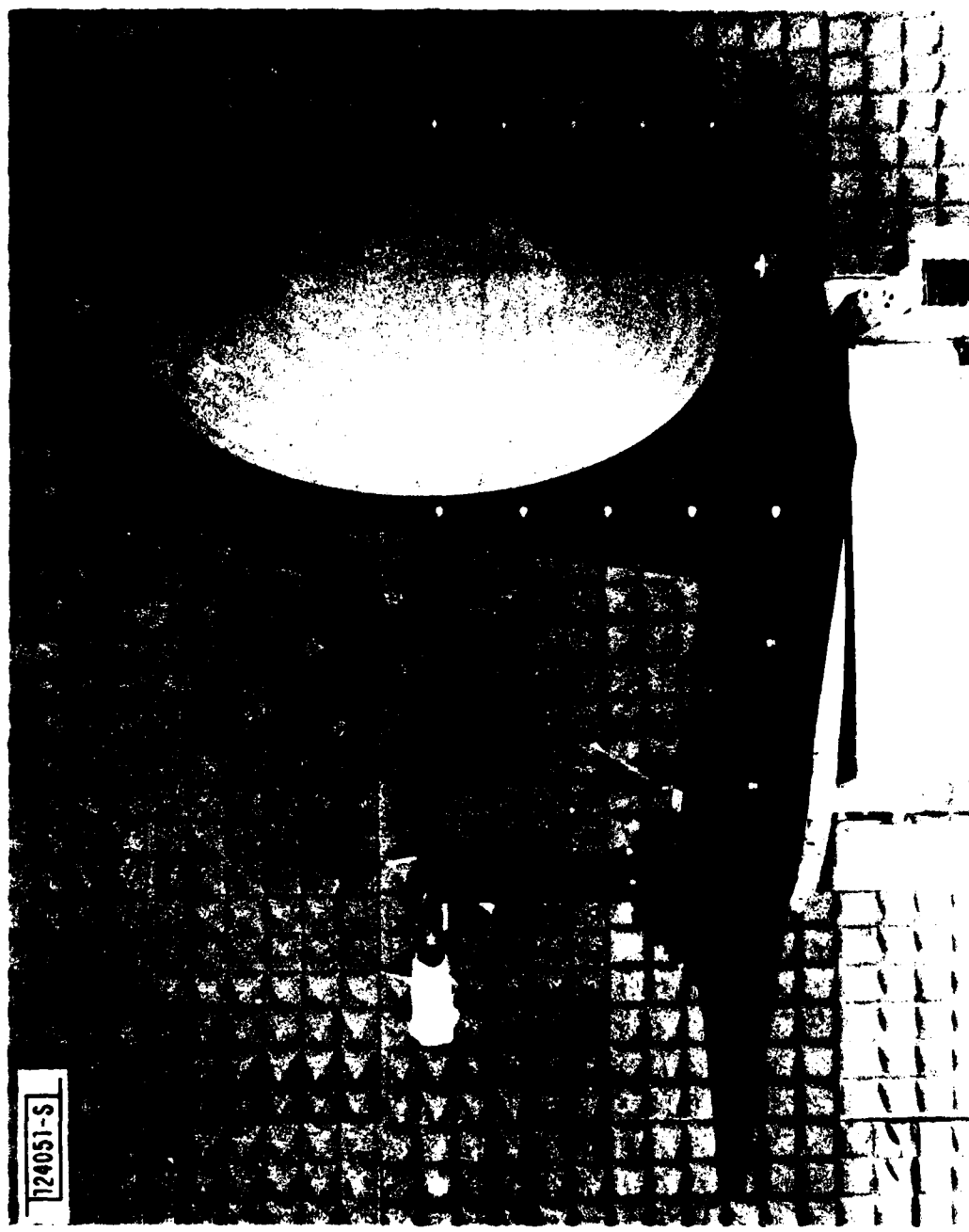
Fig. 3. Zoned dielectric lens with feed.

9
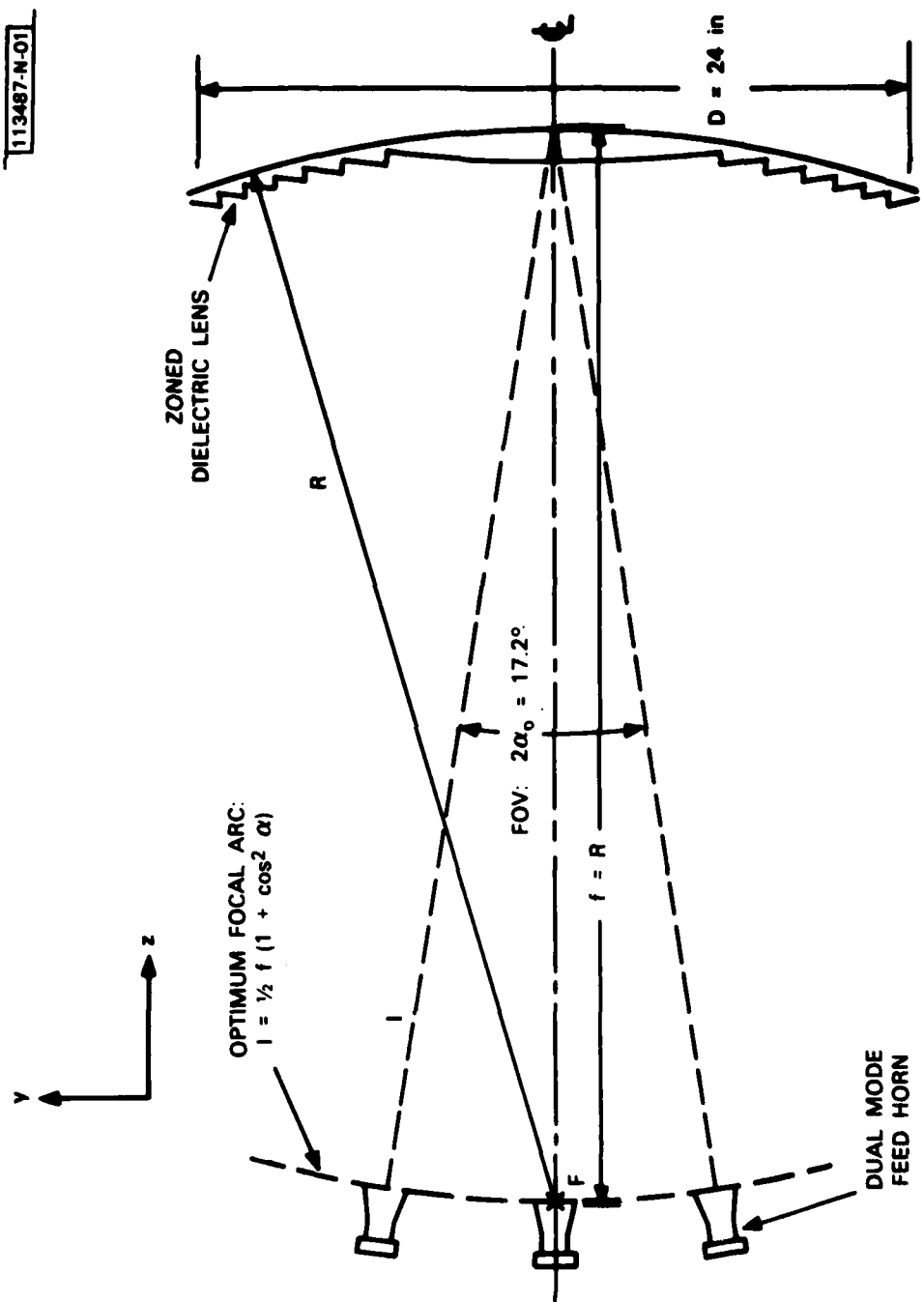
Fig. 4. EHF aplanatic dielectric lens with multiple feeds.

113487-N-01

ZONED DIELECTRIC LENS

R

FOV: $2\alpha_o = 17.2°$

f = R

OPTIMUM FOCAL ARC:
$l = \frac{1}{2} f (1 + \cos^2 \alpha)$

DUAL MODE FEED HORN

D = 24 in

F

z

y

116020-N-01

$$L1 + \mu \, L2 + L3 = CONSTANT$$
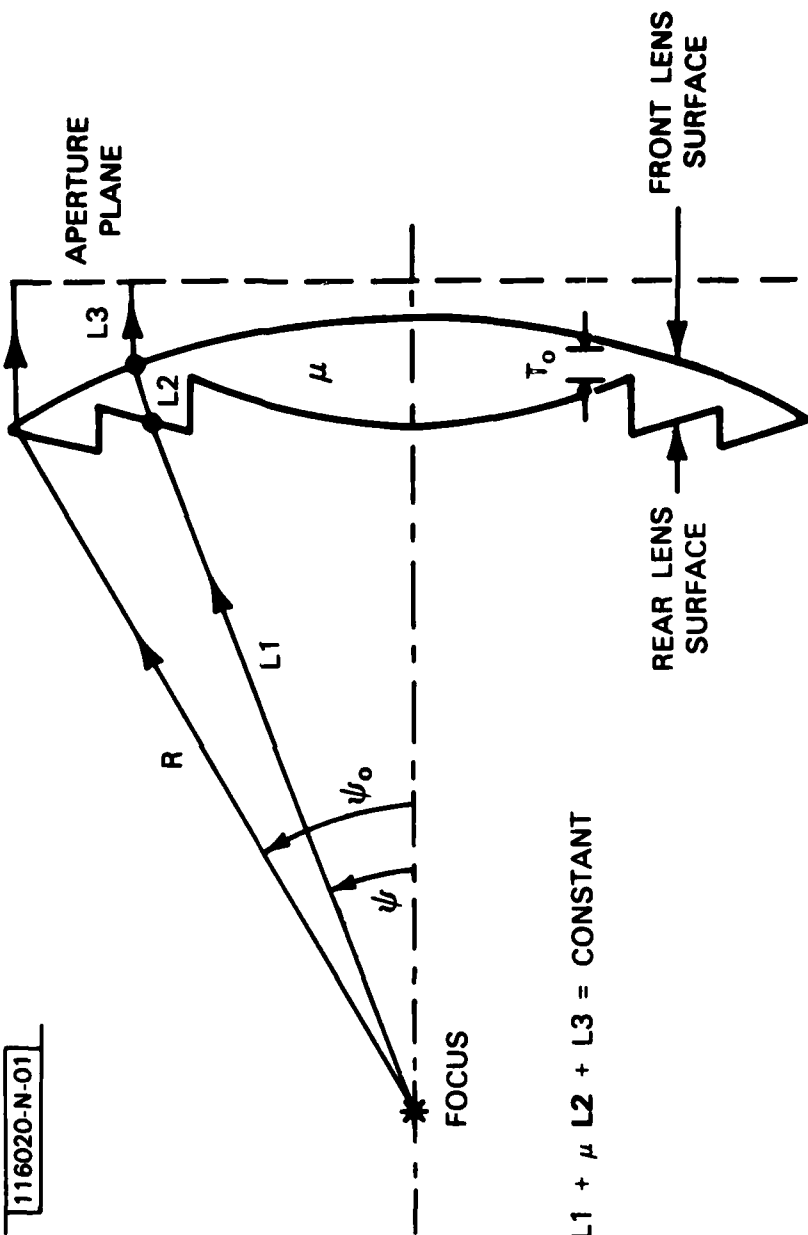
Fig. 5. Design of zoned dielectric lens.

11

III.   THIN LENS THEORY

Although the experimental lens has been designed to be without aberration for an on-axis feed at the design frequency, phase errors will occur in the wavefront of the radiated beam as it is scanned and as frequency changes. Scanning implies a linear change in the wave front as the primary feed of the lens is displaced along a focal arc. The radiated beam is then pointed approximately in the direction given by the line joining the feed to the apex of the lens. The aberrations in the phase of the wavefront cause a decrease in gain, increase in sidelobe level and broadening of the main beam of the radiation pattern. The wide angle scanning capabilities of the experimental lens may, therefore, be evaluated through the near-field determination of both phase and amplitude in the lens aperture.

A complete analysis of the lens requires consideration of the aberrations due to stepping and edge diffraction, as well as those due to the asymmetric amplitude illumination which results from scanning. This detailed evaluation is beyond the scope of the present paper. Our analysis will be restricted to geometrical optics effects for which ray-tracing is applicable. In the first approach (Method A) a ray is traced from the feed through the lens to a plane parallel to the radiated wavefront (Figure 6). The aberrations are given by the difference between the electrical path length of this ray and the principal ray which goes through the apex of the lens. [A second approach (Method B), which traces rays back from the front surface of the lens to the feed position, will be presented later in this report.]

12
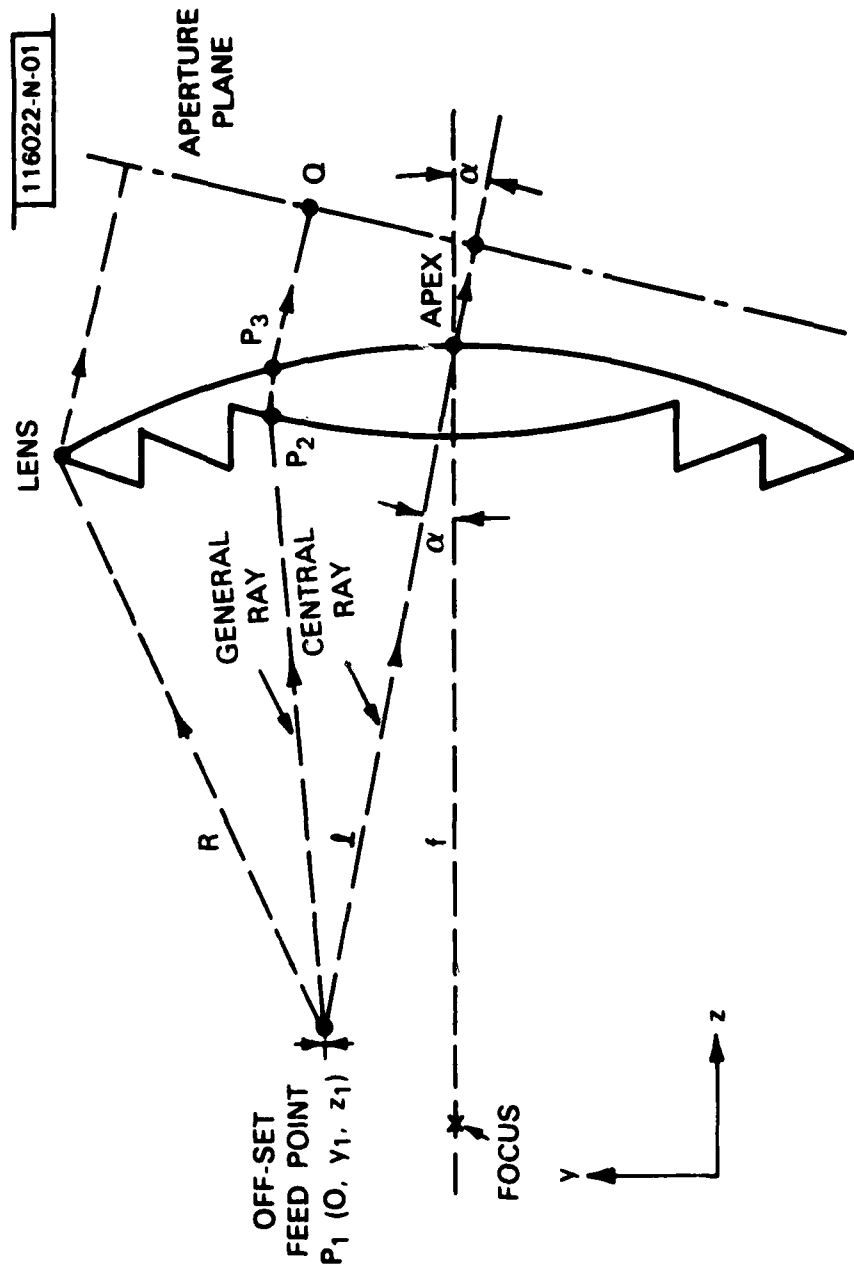
Fig. 6. Ray-trace analysis of zoned lens (Method A).

13

As a first approximation, the lens is assumed to be of zero thickness (ideally thin) so that the analysis developed in Reference 6 applies. In that paper, the wavefront aberrations, δ_n, are expressed as a power series of the x and y coordinates, measured in a plane normal to the lens axis. Only the second and third terms of the power series are considered, giving the spherical aberration, δ_2, and coma, δ_3. (The first order term is a linear beam shift. Higher order terms are negligible at small scan angles.)

Spherical aberration, δ_2, is determined by the scanning locus (focal arc) and is shown[7] to be independent of the shape of the lens. The scanning locus may always be chosen so that δ_2 is zero in any specified plane. The curvature of the scanning locus is greatest if δ_2 is reduced to zero in the plane of scan and least if δ_2 is reduced to zero in the plane orthogonal to the plane of scan.

Coma, δ_3, is mainly a function of the inner profile of the lens. A perfectly thin lens with a front surface radius R equal to its focal length f obeys the Abbe Sine condition and has minimum coma. For a lens with $F/D \geq 1.0$ and $\alpha < 30°$, the effects of coma are negligible in comparison with spherical aberration (the only remaining significant term) which is given by (Eq. 1 of Reference 7):

$$\delta_2 = \frac{1}{2}\frac{y^2}{f}(\frac{f}{\ell}\cos^2\alpha - 1) + \frac{1}{2}\frac{x^2}{f}(\frac{f}{\ell} - 1) \tag{2}$$

where (Figure 6)

   f = focal length

   ℓ = distance from scanning position to apex of lens

   α = scan angle

(The x and y coordinates of Eq. 2 are measured in an aperture plane which passes through apex of the lens and is normal to its axis of symmetry (z axis). The feed is assumed, without loss of generality, to move only in the y-z plane during scanning.)

We will now use Eq. 2 to investigate the effect of the scanning locus of the feed on δ_2. If the scanning locus is defined by

$$\ell = f \cos^2 \alpha \tag{3}$$

then $\delta_2 = 0$ in the plane of scan (y-z plane; x = 0). If it is defined by

$$\ell = f \tag{4}$$

then $\delta_2 = 0$ in the orthogonal plane (x-z plane; y = 0.) A compromise locus for the thin lens, which balances the aberrations in the y-z and x-z planes is then given by the average value of ℓ in Eqs. 3 and 4:

$$\ell = \frac{1}{2} f \left(1 + \cos^2 \alpha \right) \; . \tag{5}$$

(Equation 5 defines that scanning locus on the focal surface for which most of the experimental lens data were obtained.)

Equation 2 shows that δ_2 lacks circular symmetry since the presence of astigmatism is evidenced by the inequality of the terms involving x^2 and y^2. This fact is emphasized by writing Equation 2 for the compromise focal arc in terms of cylindrical coordinates, r and ϕ, in the x-y plane where

$$y = r \sin \phi \qquad (6)$$
$$x = r \cos \phi$$

Substituting Eq. 6 into Eq. 2:

$$\delta_2 = \frac{r^2 \sin^2\phi}{2f}\left(\frac{f}{\ell}\cos^2\alpha - 1\right) + \frac{r^2(1 - \sin^2\phi)}{2f}\left(\frac{f}{\ell} - 1\right)$$

$$= \frac{1}{2}\frac{r^2}{f}\left\{\left[\frac{f}{\ell}\left(1 - \frac{1}{2}\sin^2\alpha\right) - 1\right] + \frac{1}{2}\left[\frac{f}{\ell}\sin^2\alpha\,\cos 2\phi\right]\right\}$$

$$= \delta_s + \delta_a \qquad (7)$$

where:

$$\delta_s = \frac{1}{2}\frac{r^2}{f}\left[\frac{f}{\ell}\left(1 - \frac{1}{2}\sin^2\alpha\right) - 1\right] \qquad (8)$$

$$\delta_a = \frac{1}{4}\frac{r^2}{f}\left[\frac{f}{\ell}\sin^2\alpha\,\cos 2\phi\right] \quad . \qquad (9)$$

16

The term δ_s has circular symmetry and represents defocussing, or first order spherical aberration, while δ_a is asymmetrical and represents astigmatism. (These definitions are in accordance with the classification of the primary (Seidel) aberrations[9], but are at variance with those used in Reference 7.)

The maximum aberrations for a given scan angle, α, are obtained at the edge of the lens for which r equals the lens radius a. Then, Eqs. 8 and 9 become

$$(\delta_s)_{max} = + \frac{a^2}{2f}\left[\frac{f}{\ell}\left(1 - \frac{1}{2}\sin^2\alpha\right) - 1\right] \tag{10}$$

$$(\delta_a)_{max} = + \frac{a^2}{2f}\left[\frac{f}{\ell}\left(\sin^2\alpha\,\cos 2\phi\right)\right] \tag{11}$$

$a = D/2 = $ lens radius.

We will now consider the phase aberrations (Eqs. 8 and 9) associated with four specific scanning loci (Figure 7).

Case 1 (Circular locus with center at apex of lens):

$$\ell = f \tag{12}$$

$$\delta_s = -\frac{1}{4}(r^2/f)\,(\sin^2\alpha) \tag{13}$$

$$\delta_a = +\frac{1}{4}(r^2/f)\,(\sin^2\alpha\,\cos 2\phi) \tag{14}$$

17

116019-N-01

FRONT
LENS
SURFACE

FOCAL ARCS

A

B

C

D

L

F

R

α

FOCUS
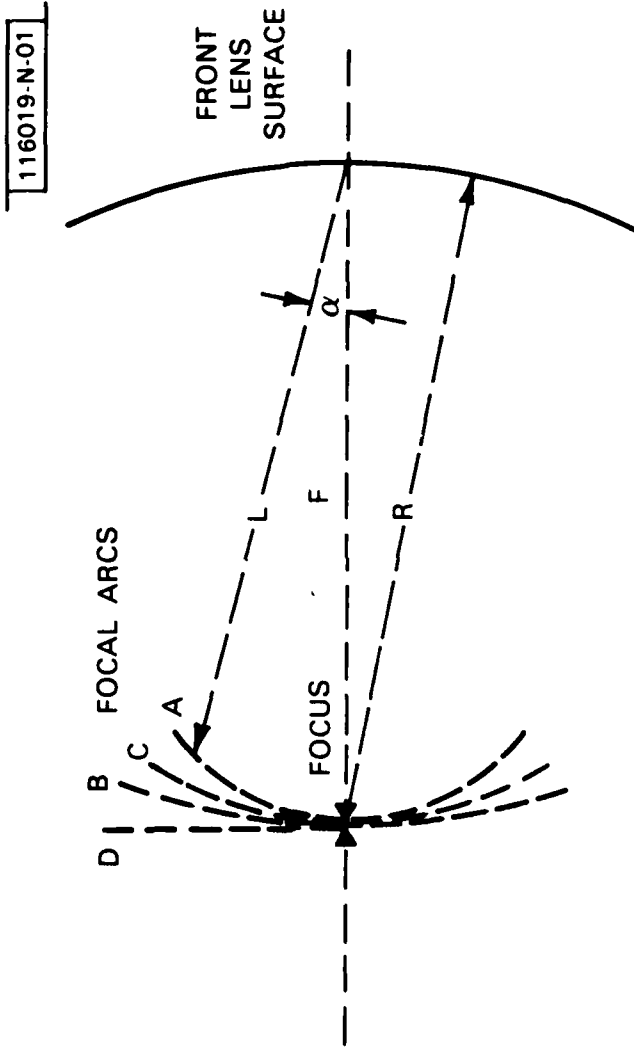
Fig. 7. Representative focal arcs for thin dielectric lenses.

18

The phase aberrations are divided equally, in this case, between astigmatism and first order spherical aberration.

Case 2 (Flat focal plane):

$$\ell = f/\cos\alpha \tag{15}$$

$$\delta_s = -\frac{1}{2}(r^2/f)\left[1 - \frac{1}{2}(\cos\alpha + \cos^3\alpha)\right] \tag{16}$$

$$\delta_a = +\frac{1}{4}(r^2/f)\left[(\cos\alpha - \cos^3\alpha)(\cos 2\phi)\right] \tag{17}$$

Case 3 (Eq. 3):

$$\ell = \cos^2\alpha \tag{18}$$

$$\delta_s = +\frac{1}{4}\left(\frac{r^2}{f}\right)\left[\tan^2\alpha\right] \tag{19}$$

$$\delta_a = +\frac{1}{4}(r^2/f)\left[\tan^2\alpha \cos 2\phi\right] \tag{20}$$

Case 4 (Compromise focal arc):

$$\ell = \frac{1}{2}(\cos^2\alpha + 1)f \tag{21}$$

$$\delta_s = 0 \tag{22}$$

$$\delta_a = \frac{1}{2}(r^2/\ell)\left[\frac{\sin^2\alpha}{1 + \cos^2\alpha}\right][\cos\ 2\phi] \tag{23}$$

The primary spherical abberation term δ_s has therefore vanished in this latter case, leaving only the astigmatism term δ_a. Note that, in all four cases, the astigmatism term varies only slightly while primary spherical aberration depends strongly on the curvature of the focal arc. This can be seen by calculating the maximum spherical and astigmatic aberrations $(\delta_s)_{max}$ and $(\delta_a)_{max}$ from Eqs. 10 and 11 for the above cases, using the experimental lens parameters (Table I: $\alpha = 9°$; $F/D = 1.5$; $D = 90\lambda$).

TABLE I

SCANNING ABERRATIONS FOR EXPERIMENTAL LENS PARAMETERS

Case	ℓ/f	$(\delta_s)_{max}/\lambda$	$(\delta_a)_{max}/(\lambda \cos 2\phi)$
1	1.0000	−0.092	+0.092
2	1.0124	−0.183	+0.091
3	0.9755	+0.094	+0.094
4	0.9877	0	+0.093

IV. PHASE ERRORS IN ZONED LENSES

The zoned lens can be considered to be a reasonable approximation to the thin lens with respect to phase aberrations over its aperture. The major difference is that a frequency-dependent phase error term δ_f is introduced due to the zoning. This effect will now be evaluated by comparing ray path calculations in the zoned lens with the approximate thin lens results derived in the last section.

The frequency sensitivity of the lens can be derived approximately for the on-axis case by noting that path length discontinuities of one wavelength occur at each step. Since the phase is modulus 2π, this does not result in any phase error at the design wavelength λ_0 for an on-axis feed. However, at any other wavelength λ, the path length error $\Delta\ell_T$, relative to the central ray, is given by:

$$\Delta\ell_T/\lambda \triangleq \delta_f/\lambda = \left(\frac{\lambda_0}{\lambda} - 1\right)n \qquad (24)$$

where n is the step number (starting from the center of the lens). Figure 8 shows this path length error for the experimental lens at the band extremities (43.5 and 45.5 GHz), both as a discontinuous curve with phase jumps at the steps and as a continuous approximation. (The position of the steps are obtained from Appendix A). We will show that the total phase (path length) errors in the zoned lens can be obtained approximately by adding this frequency-dependent term δ_f to the thin lens values, δ_g and δ_a.
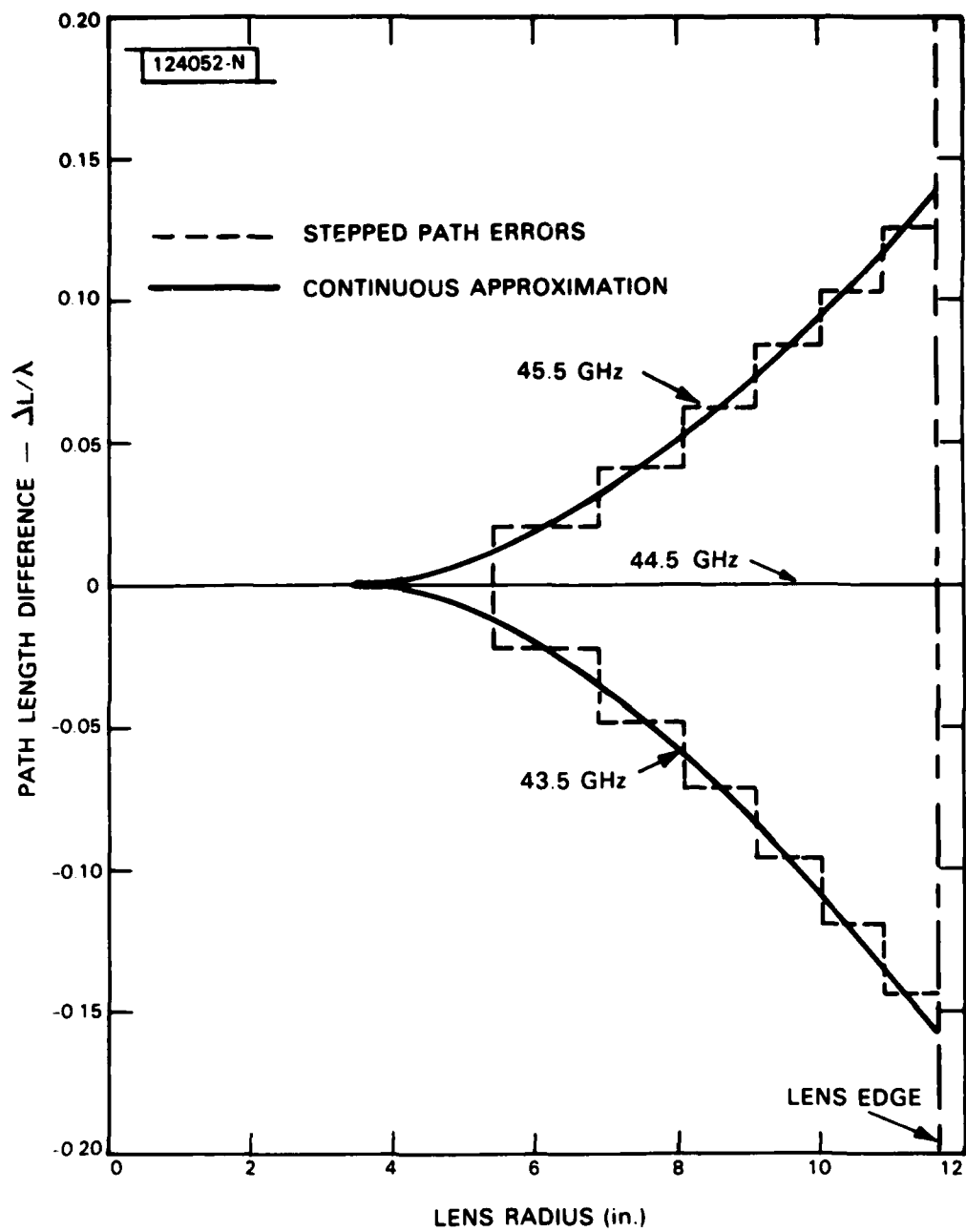
Fig. 8. Frequency-dependent component, δ_f, of lens path length error.

The equations used in Method A to trace rays from an arbitrary feed position through the lens to the aperture plane and to determine the resultant path length differences are presented in Appendix B. In this approach (Figure 6), the feed is assumed to lie in the y-z plane at a position $P_1(0, y_1, z_1)$. [The (x, y, z) coordinate systems have their origins at the apex of the lens.] The ray under consideration intersects the rear surface of the lens at a specified point $P_2(x_2, y_2, z_2)$ or, in cylindrical coordinates, $P_2(r, \phi, z_2)$. Snell's law then determines the refraction of the ray at this surface and its subsequent intersection with the front lens surface (a sphere with defining equation $[x^2 + y^2 + (R + z)^2] = R^2$) at the point $P_3(x_3, y_3, z_3)$. From here, the ray is assumed to be normally incident upon the wavefront reference plane which is orthogonal to the beam direction. (This last step is a simplifying assumption which is valid, in accordance with Fermat's principle, for small path length errors.) The total path length ℓ_T is calculated from the three ray components:

$$\ell_T = \ell_1 + \mu\ell_2 + \ell_3 \tag{25}$$

where

$\ell_1 = \overrightarrow{P_1 P_2}$ = distance from feed to rear lens surface,

$\ell_2 = \overrightarrow{P_2 P_3}$ = distance from rear to front lens surfaces,

24

$\ell_3 = \overrightarrow{P_3 0}$ = distance from front lens surface to output reference plane,

μ = index of refraction of lens dielectric,

The path length difference $\Delta\ell_T$ is then obtained as the difference between ℓ_T for the general ray and that for the central ray, which passes through the apex of the lens.

These normalized path length differences $(\Delta\ell_T/\lambda)$ are plotted in Figure 9 as a function of radial distance from the apex of the lens for a feed which is located on the compromise scanning locus $[\ell = 1/2(\cos^2\alpha + 1)f]$ for both on-axis ($\alpha=0°$) and off-axis ($\alpha = 8.6°$) positions. The solid curves are the computer outputs from the ray tracing program while the dashed lines are the thin lens approximations, including the frequency-dependent term δ_f, from Eqs. 23 and 24 ($\delta_2 = \delta_a + \delta_f$; $\delta_s = 0$). The calculations are shown for three different cuts through the aperture plane of the lens ($\phi = 0°$, 45°, 90°) and for three frequencies (43.5, 44.5 and 45.5 GHz). In the thin lens approximation the path length error is zero over the aperture (Figure 9e) for the on-axis ($\alpha = 0°$) feed position at the design frequency (44.5 GHz). At all frequencies the astigmatism term δ_a disappears for both the on-axis case (Figures 9a, e, i) and the $\phi = 45°$ cuts (Figures 8c, g, k), leaving only the frequency-dependent term δ_f. Likewise, δ_f is zero at the design frequency for any feed position, leaving only astigmatism (Figures 9e, f, g, h). Both the frequency and astigmatism terms are present at frequencies other than the design frequency for the off-axis feed in the principal planes ($\phi = 0°$ and 90°; Figures 9b, d, j, ℓ). It can be seen that the thin lens approximations

25
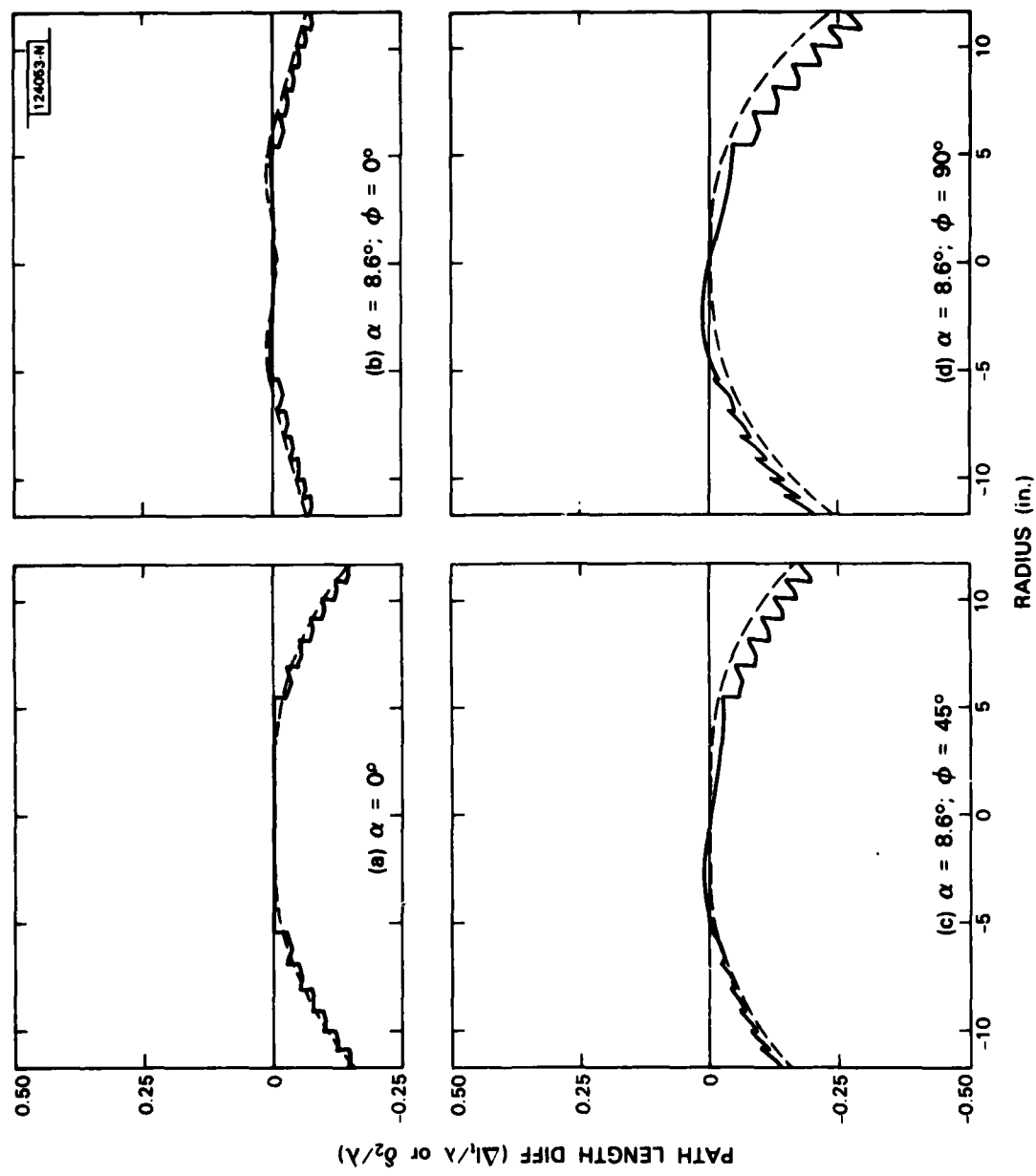
Fig. 9(a–d). Path length errors in zoned lens. 43.5 GHz.

26

Fig. 9(e–h) 44.5 GHz.

27

Fig. 9(1-1)   45.5 GHz.

28
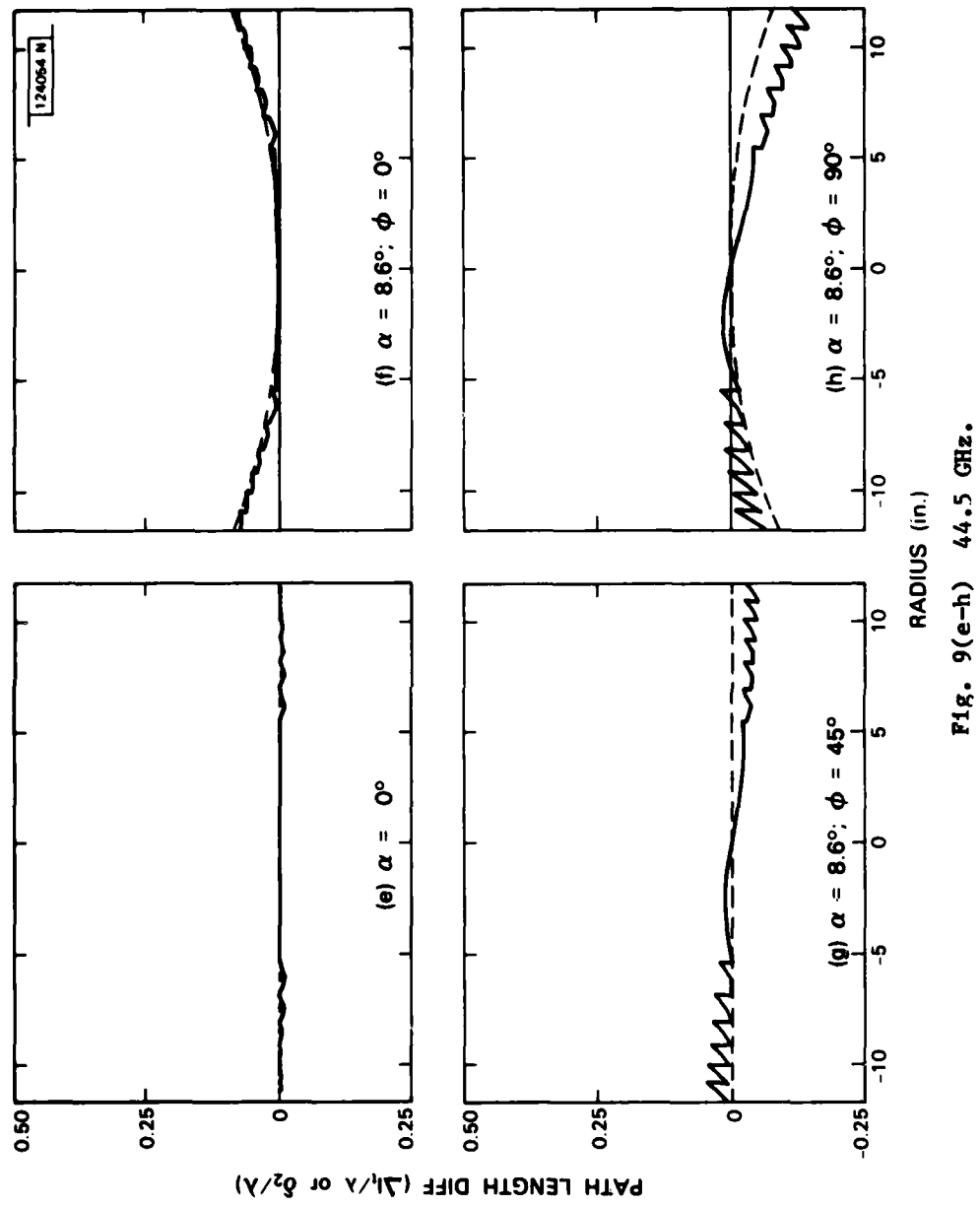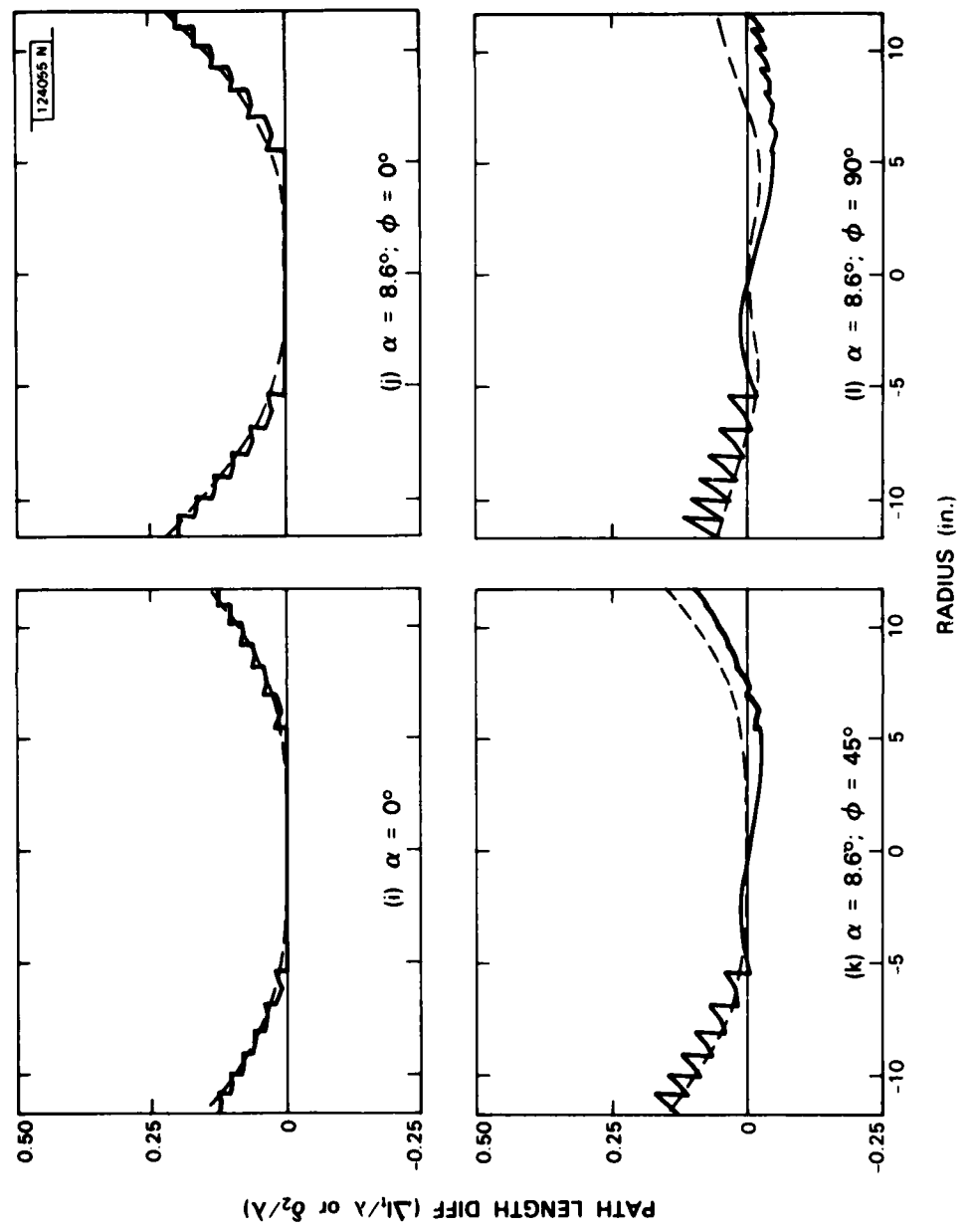
lens approximations follow the trends of the ray trace results in all cases
and could be used to predict the radiation characteristics of the lens design
with reasonable accuracy and a minimum amount of computation.

V. EFFECTS OF BEAM SCANNING ON RADIATION PATTERNS

The far-field radiation patterns of the zoned lens were calculated by two different techniques. In Method A (Fig. 6) the fields are integrated over a circular aperture in the plane normal to the beam direction. This procedure makes use of the output of the ray trace program discussed in the previous section. In the second approach (Method B) the rays are traced backwards from the spherical front lens surface to the feed (Figure 10; P_3 to P_2 to P_1). The intensity of illumination over this surface is then evaluated from the power contained within ray bundles emanating from the feed. Finally, the far-field radiation patterns are computed by an integration over the lens surface. Typical radiation pattern and gain computations obtained by both of these methods are now presented for comparison with experimental results and with the thin lens approximations.

In Method A the far-field, unnormalized, radiation pattern $F(\theta',\phi')$ of a circular aperture of radius a in a plane is given by[10]:

$$F(\theta',\phi') = \int_0^a dr \int_0^{2\pi} d\phi \; E(r,\phi) \; \exp\{jkr \sin\theta' \cos(\phi' - \phi)\} \qquad (26)$$

where $k = 2\pi/\lambda$.

Here, $E(r,\phi)$ is evaluated at the lens aperture coordinates (r, ϕ) while the far-field amplitude $F(\theta',\phi')$ is evaluated at the polar coordinates (θ',ϕ') where θ' and ϕ' are measured in a coordinate system oriented relative to the beam direction (Figure 11). The complex amplitude $E(r,\phi)$ can be written in the form:

30

116023-N-01

FIELDS INTEGRATED
OVER FRONT LENS
SURFACE

LENS

P₃

P₂

P₁ (O, y₁, z₁)

TE₁₁ MODE
WAVEGUIDE

α

β

FOCUS

Y

z

α = LENS SCAN ANGLE
β = FEED POINTING ANGLE
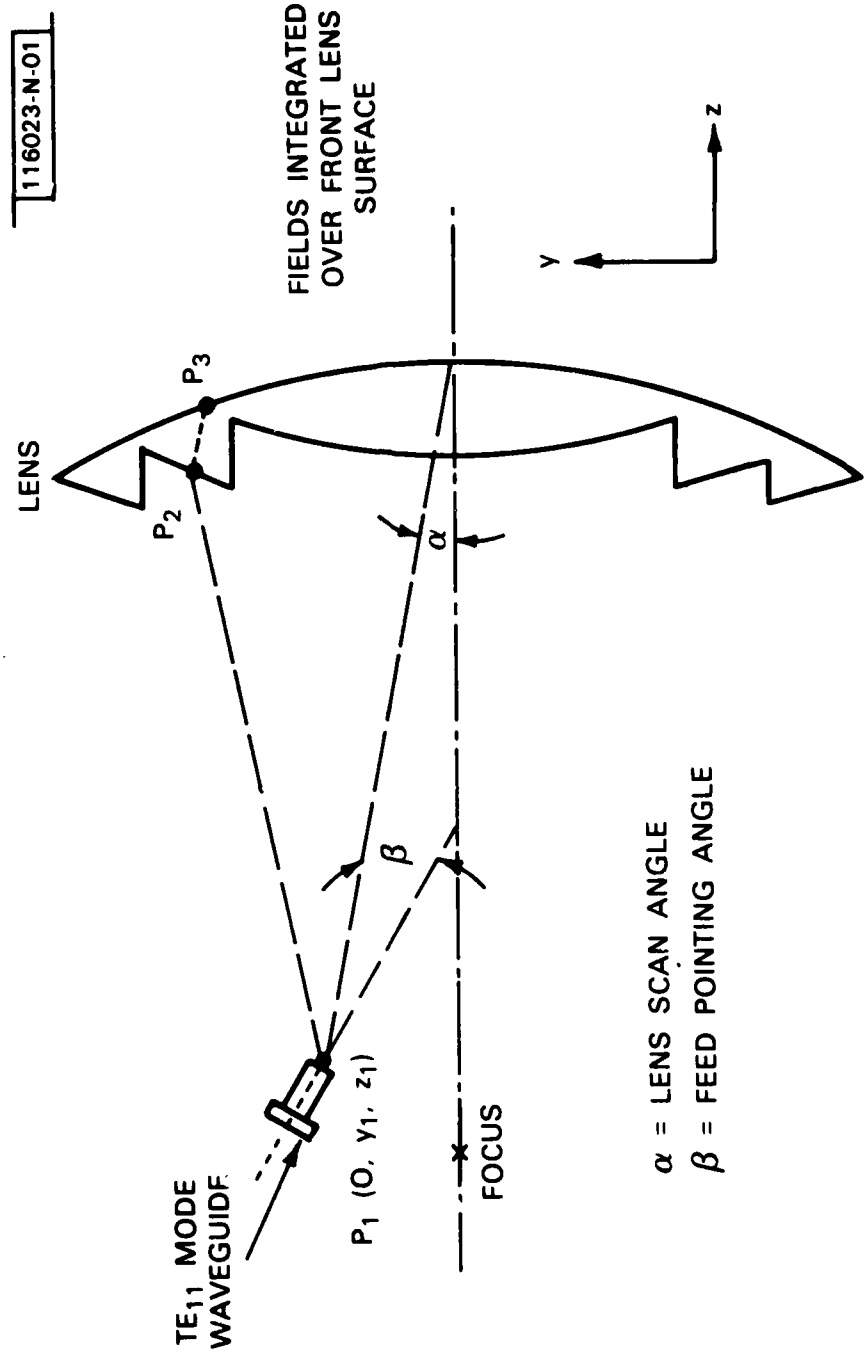
Fig. 10. Stationary optical path analysis of zoned lens (Method B).

31
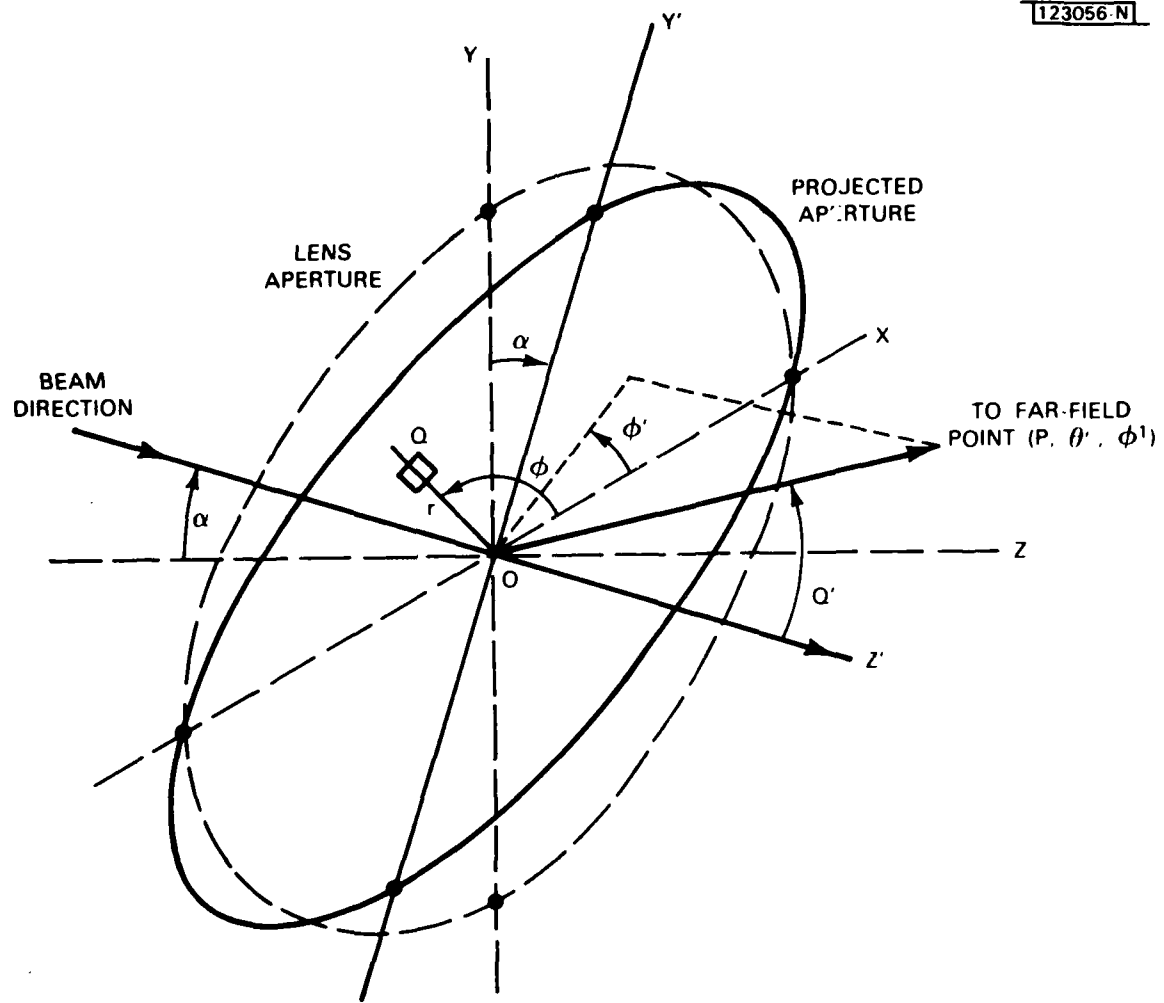
Fig. 11. Coordinate system for far-field calculations.

$$E(r,\phi) = E_m(r,\phi) \, e^{j\beta(r,\phi)} \tag{27}$$

where $E_m(r,\phi)$ is the magnitude of the aperture field and the constant $\beta(r,\phi)$ is determined from the path length differences of the rays as

$$\beta(r,\phi) = 2\pi \, (\Delta \ell_T)/\lambda \tag{28}$$

Under the assumption that the aperture illumination function is circularly symmetrical $[\,|E(r,\phi)| = E_m(r)\,]$, the directive gain $G(\alpha)$ may be obtained by an integration over the aperture plane:

$$G(\alpha) = \left[8/\lambda^2 \right] \frac{\left| \int_{-\pi/2}^{\pi/2} \int_0^a E(r,\phi) \, r \, dr \, d\phi \right|^2}{\int_0^a |E(r,\phi)|^2 r \, dr} \tag{29}$$

(Alternatively, the gain may be computed by integrating the far-field radiation patterns.) Details of the pattern and gain integration procedures are presented in Appendix C.

Typical radiation patterns, calculated from Equation 26, are shown in Figure 12 for an assumed aperture distribution of the form

$$|E(r,\phi)| = E_o\left(1 - \frac{2}{3}\, \hat{r}^2\right) \tag{30}$$

33
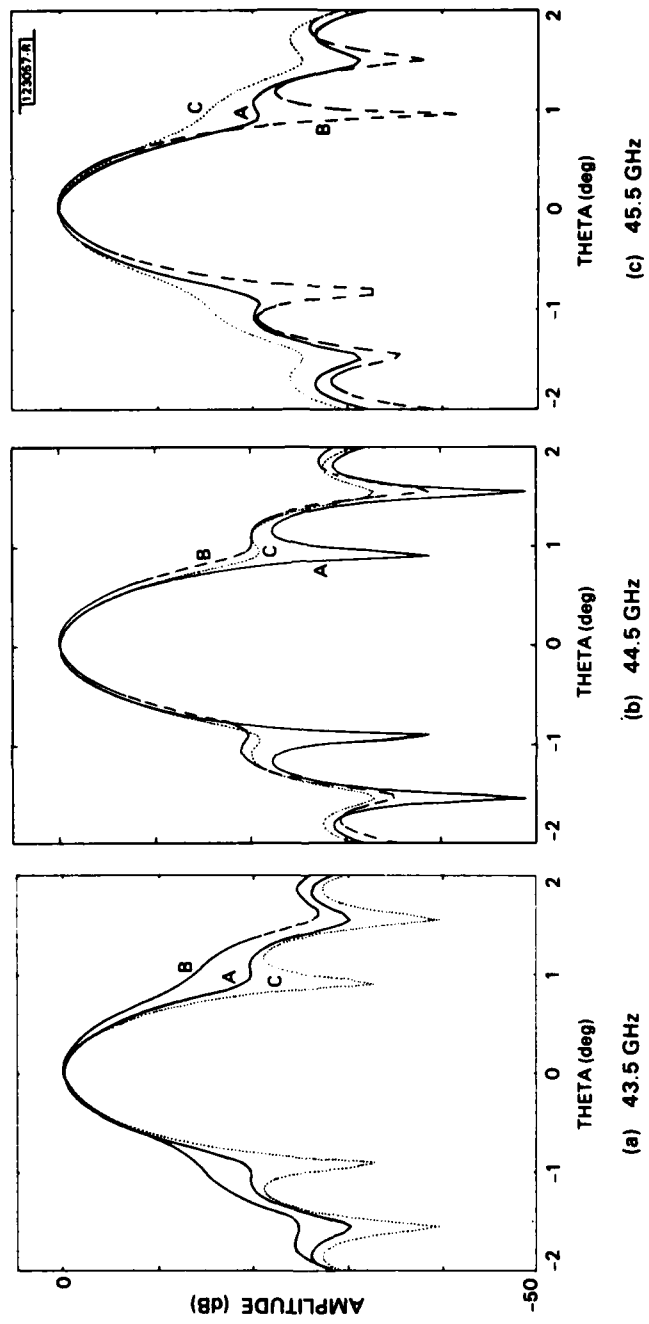
Fig. 12(a-c)   Theoretical radiation patterns of zoned lens: 45.5 GHz
[Curve A: $\alpha = 0°$; Curve B: $\alpha = 8.6°$, $\phi' = 90°$; Curve C: $\alpha = 8.6°$, $\phi' = 0°$]

where $\tilde{r}$ is the normalized lens radius[*]. For the feed on-axis ($\alpha = 0°$), the patterns exhibit the sharp nulls and low sidelobes at the design frequency (44.5 GHz) which are expected from a uniform phase distribution, while showing wider main beams, fill-in of the first nulls, and higher sidelobes at the band edges (43.5 and 45.5 GHz). This pattern degradation is evidence for the existence of frequency-dependent phase errors. (Compare curves A of Figs. 12a, b, c with the corresponding phase error curves of Figures 9a, e, i.) Similarly, the principal plane cuts in the radiation pattern for the off-axis feed position ($\alpha = 8.6°$; $\phi = 0°$ and $\phi' = 90°$; Curves B and C in Fig. 12b) are essentially identical to each other at the design frequency since the phase errors due to astigmatism are almost equal in both planes and no other phase errors are present.

The situation becomes more complicated for the off-axis feed and at the frequency extremes since both *frequency-independent* and *scan-dependent* phase errors are simultaneously present, and they can tend either to reinforce or cancel each other. At the lower end of the band (43.5 GHz), the beam is well focussed in the orthogonal plane ($\phi' = 0°$), where the phase errors tend to cancel, and defocussed in the scan plane ($\phi' = 90°$), where the errors add. These effects are reversed at the upper frequency limit (45.5 GHz) where the beam is well focussed in the scan plane and defocussed in the orthogonal plane (See Figs. 12a, 12c, 9b, 9d, 9j, and 9ℓ.) The reason for this reversal is the

---

[*]Equation 30 is the same illumination function which was assumed in References 3 and 7 for the evaluation of scanning losses and performance of a lens antennas. It is a first-order approximation to the lens illumination produced by a feed horn, which would actually vary as a function of feed position on the scan locus and would generally be asymmetrical.

change in sign of the frequency-dependent phase error (Eq. 24) between the lower and upper frequency limits. These comparisons show that the thin lens equations provide a reasonable and rapid estimate of the radiation characteristics of the zoned lens, as an alternative to the more accurate but more complex ray trace calculations.

The radiation patterns of the lens were measured over a 43.5 to 45.5 GHz frequency range, using two different feed horns. These feeds (Figure 13) are scaled models of a dual-mode conical horn (shown in Figure 12 of Reference 11), designed for equal beamwidth in its E and H planes. The radiation patterns of this type of feed horn are designed to be circularly symmetrical and essentially identical to the H-Plane pattern of an open-ended circular waveguide carrying the TE_{11} mode[12].

E and H plane measured patterns of the short horn (Figure 13a; r = 0.403 in) are shown in Figure 14 for 44.5 GHz and 45.5 GHz. The theoretical H-plane radiation patterns of a circular waveguide of the same radius as the horn are also shown for comparison. Since this short feed horn produces an aperture illumination of the lens with an edge taper on the order of 8 dB, which is reasonably close to the 10 dB value for the theoretical lens illumination function $[E(r) = 1 - (2/3) r^2]$, the comparisons between the theoretical and experimental lens patterns will generally be presented for this feed only. (The long feed horn (Figure 13b) has an aperture radius of 0.568 in and produces a lens edge taper of about 19 dB). The short feed horn is relatively narrow band since the E and H plane primary patterns change with

36

ALL DIMENSIONS IN INCHES

123058-N
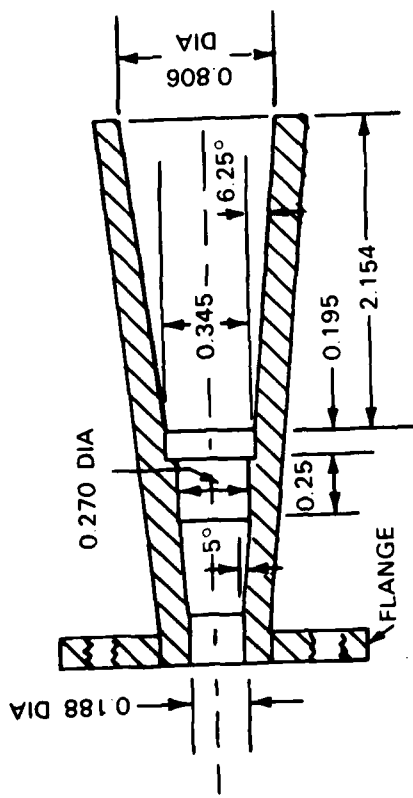
(a) SHORT HORN (r = 0.403 in.)
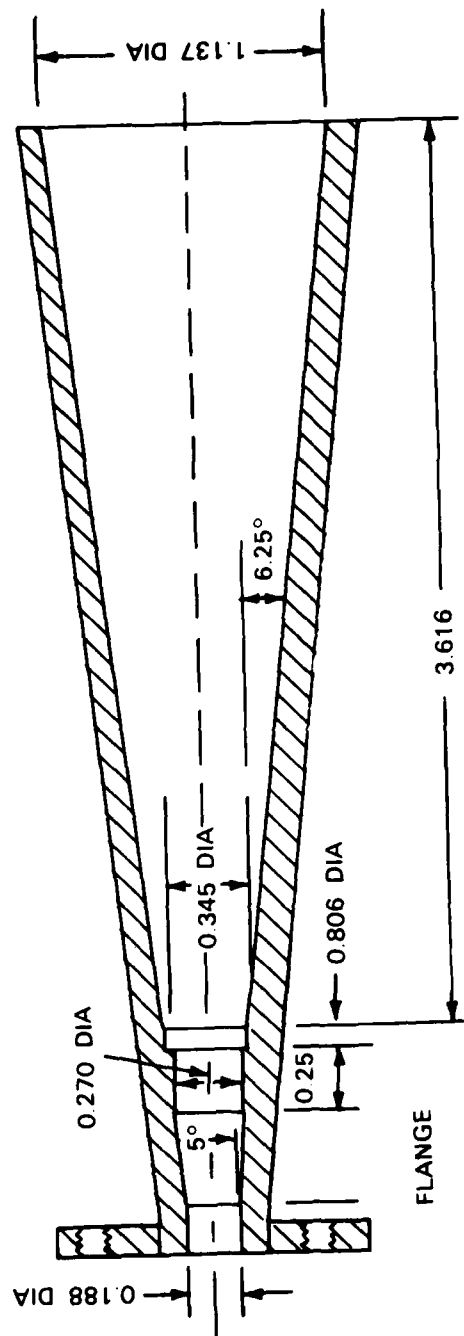
(b) LONG HORN (r = 0.568 in.)

Fig. 13. Feed horn dimensions.

37
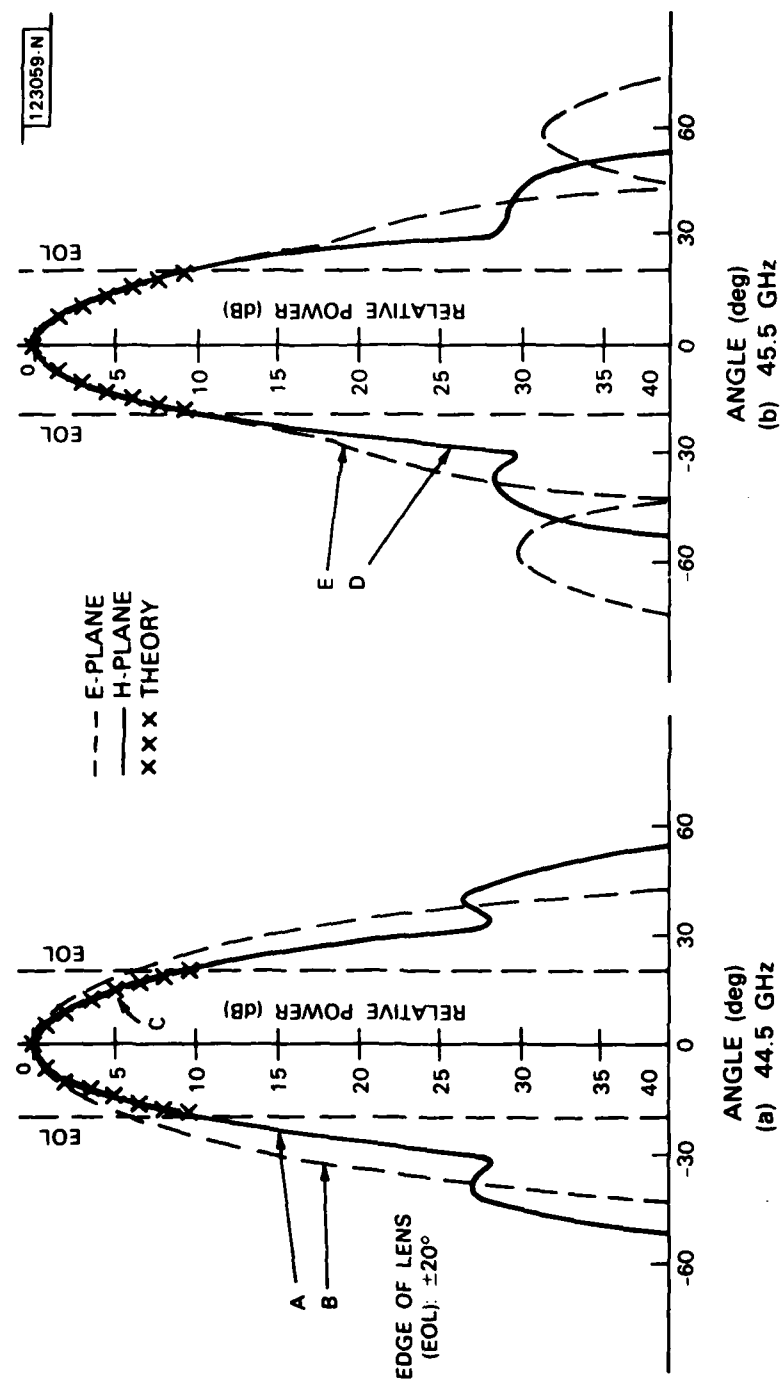
Fig. 14. Primary radiation patterns of short horn.

38

frequency, being more nearly equal at 45.5 GHz (Figure 14b) than at the 44.5 GHz design frequency (Figure 14a). (These patterns differed sufficiently at 43.5 GHz so that this frequency was not used in the analysis of lens performance.)

The on-axis ($\alpha = 0°$) radiation patterns of the lens were calculated for the two different feed horn radii (0.568 in and 0.403 in), using both the ray trace technique (Method A) and the stationary phase method (Method B). In the Method A computations, the feed illumination was assumed to be circularly symmetrical* while, in Method B, the illumination was chosen to be equivalent to that for the non-symmetrical TE_{11} mode in circular waveguide. The measured on-axis radiation patterns of the lens with the short feed horn are compared in Figure 15 at 44.5 GHz with the results obtained by both Methods A and B. Very close agreement is obtained for all three results, including the details of main and sidelobe structures. Similar good results between the measurements and Method A are obtained for the long horn (Fig. 16). However, the lens radiation patterns with the short horn have higher first sidelobes (25 dB versus 33 dB) and a narrower main beam than those for the long horn. This is to be expected since the short horn has the smaller lens amplitude taper (8 dB versus 19 dB).

Since the feed patterns were not circularly symmetrical except at 45.5 GHz, the on-axis lens patterns were different for the E and H planes.

---

*The circularly symmetrical feed illumination was chosen, in this case, as the H-plane pattern of a circular waveguide operating in the TE_{11} mode. This required a modification of the Method A computer programs which previously used Eq. 33 as the lens illumination.
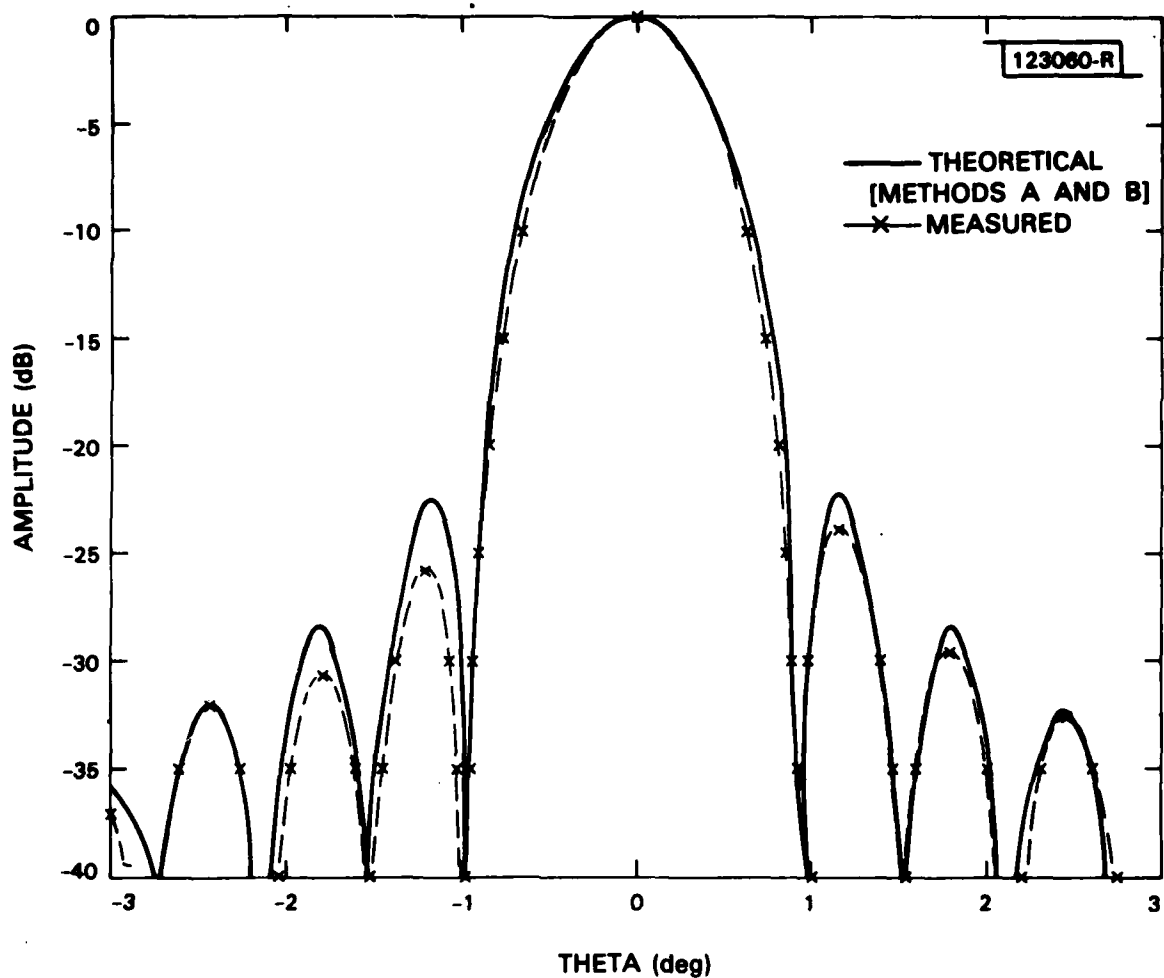
Fig. 15. On-axis radiation patterns of zoned lens with short horn (44.5 GHz).

40
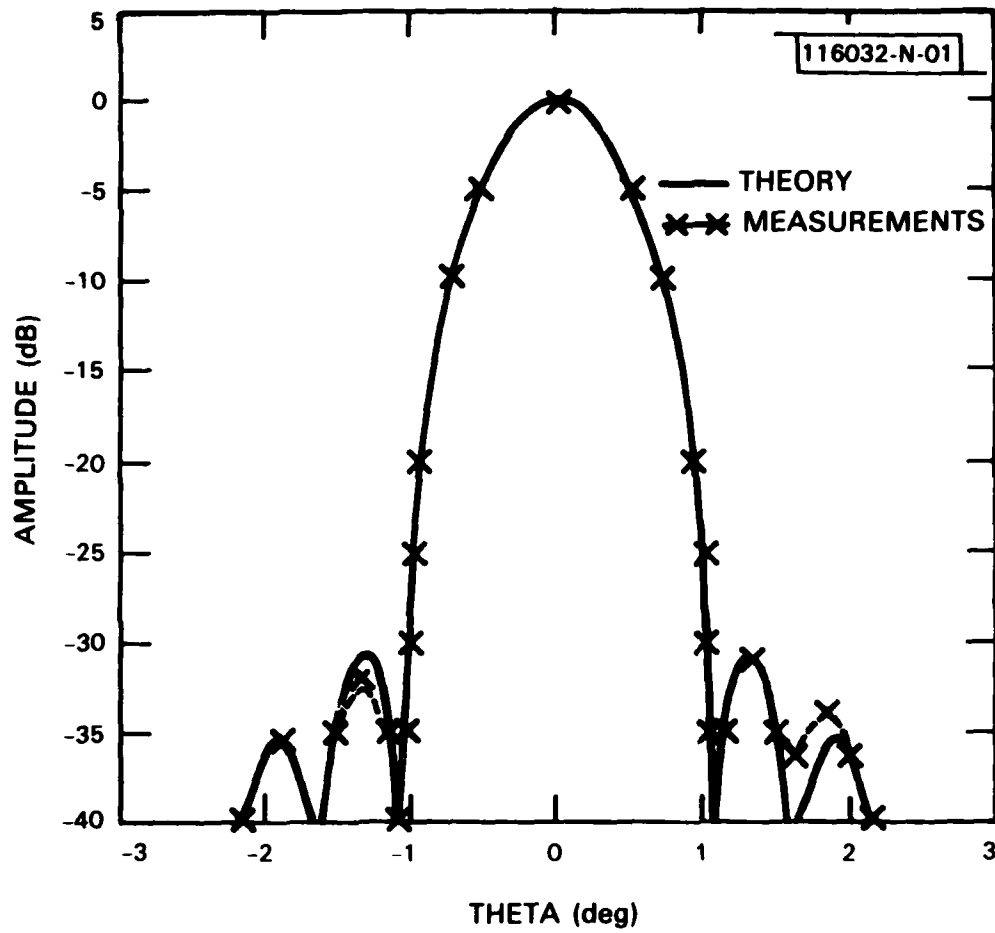
Fig. 16. On-axis radiation patterns of zoned lens with long horn (44.5 GHz).

41

Despite this variance close agreement was obtained in all on-axis cases between the results of the analyses and the experimental H-plane patterns. (However, the measured gain would not be expected to agree with the calculations of either Method A or B since their theoretical and measured lens illumination functions are different.)

The off-axis radiation patterns ($\alpha = 8.6°$) could not be computed by Method A (in its present form) with high accuracy for two reasons. First, Method A assumes a rotationally symmetrical lens illumination whereas an off-axis feed produces an asymmetrical illumination which depends upon the variable distance from the feed to different points on the lens. Second, the illumination depends on the orientation of the feed (which may not be pointed at the apex of the lens), as well as on its position. However, both of these effects are taken into account by Method B, which calculates power flow from the feed through the lens system and provides absolute gain values (including spillover effects), rather than directive gain, for the far-field patterns.

The off-axis radiation pattern of the lens, measured in the plane of scan ($\alpha = 8.6°$; $\phi' = 90°$) at 44.5 GHz, is compared in Figure 17 with the results predicted by Method B. (These curves should also be compared with the curve B of Figure 12b, which were derived by Method A.) Reasonable agreement is obtained; both the measurements and theory show broadening of the main beam and the blending of the first sidelobe into a main beam shoulder. Measured radiation patterns are also shown in Figure 18 for both on-axis ($\alpha = 0°$) and off-axis ($\alpha = 8.6°$; $d' = 0°$ and $90°$) cuts at 45.5 GHz. These results confirm qualitatively the predictions of Figure 12c which show similar features,

42
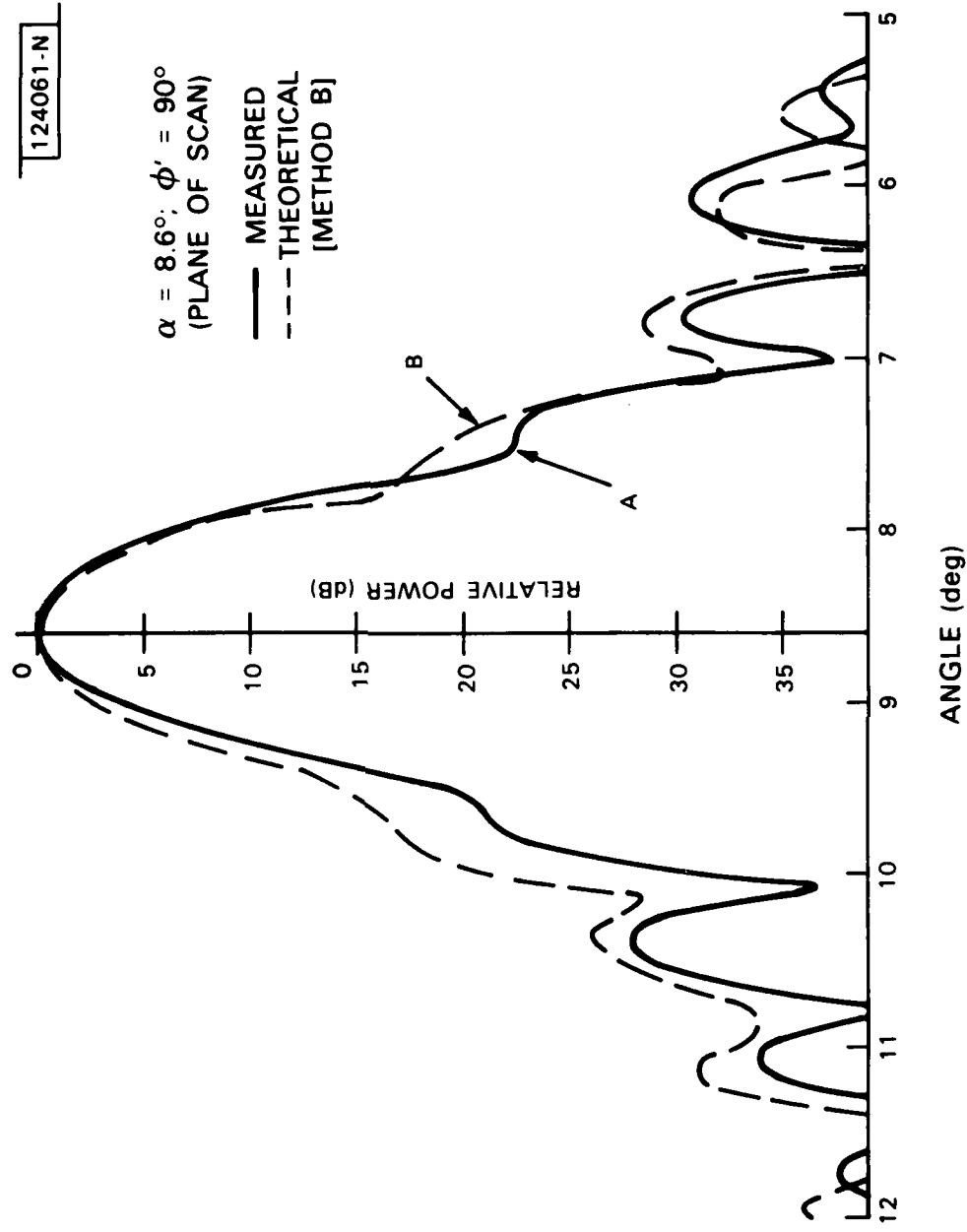
Fig. 17. Off-axis radiation patterns of zoned lens (44.5 GHz).

43
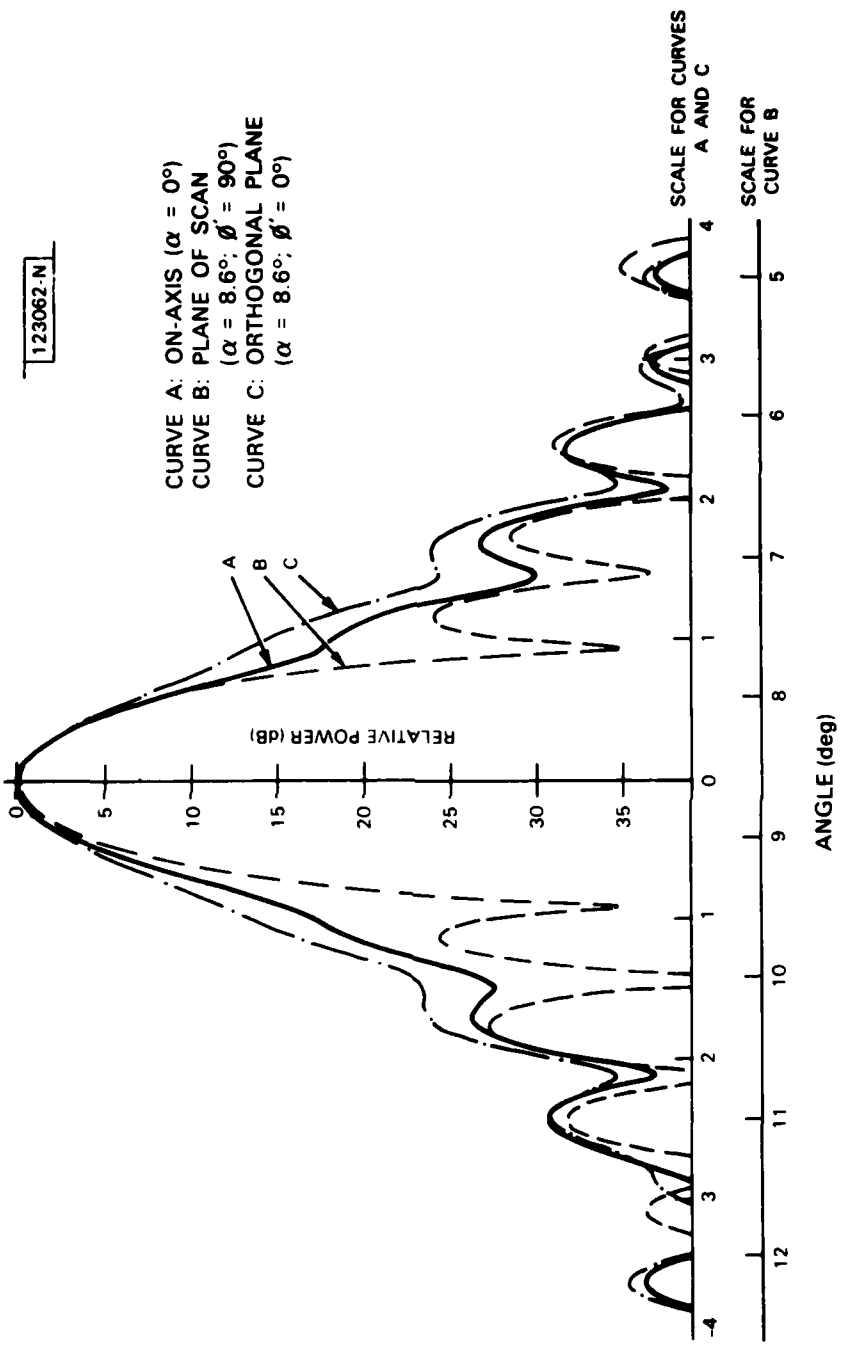
Fig. 18. Measured radiation patterns of zoned lens (45.5 GHz).

44

including on-axis frequency-dependent defocussing and a highly focussed pattern in the plane of scan.

For both the measured and theoretical radiation patterns which have been presented to this point, the feed horn was pointed at the apex of the lens. However, this orientation may not be practical in multibeam applications where many feed horns are clustered over the focal surface. The effects of pointing the feed horn away from the apex of the lens was, therefore, investigated by moving the feed horn to an off-axis position (α = 8.7°) on the compromise feed locus and then tilting the horn by an angle β (Figure 10) in 5° steps about the nominal beam direction for a maximum excursion of $\pm$ 10°. (Each 5° step corresponds to a shift at the position of maximum intensity of the aperture illumination from the center of the lens by approximately three inches in the plane of scan.) The resultant radiation patterns for each step position are shown for cuts in both the plane of scan (Figure 19; ϕ'= 90°) and the orthogonal plane (Figure 20; ϕ' = 0°). The principal effect which is observed is a reduction in the gain at the peak of the beam by about 1.3 dB at the extremes of the horn tilt (β = $\pm$ 10°). The radiation patterns become asymmetrical in the plane of scan with increasing tilt angle, broadening principally in that side of the lens towards which the feed horn is tilted. However, the radiation patterns in the orthogonal plane change only slightly; for both planes, the beamwidths down to about the −10 dB level remain invariant with tilt angle. These observations are consistent with the hypothesis that the decrease in peak gain is due primarily to spillover effects (where the radiation from the feed misses the lens surface) and that

45
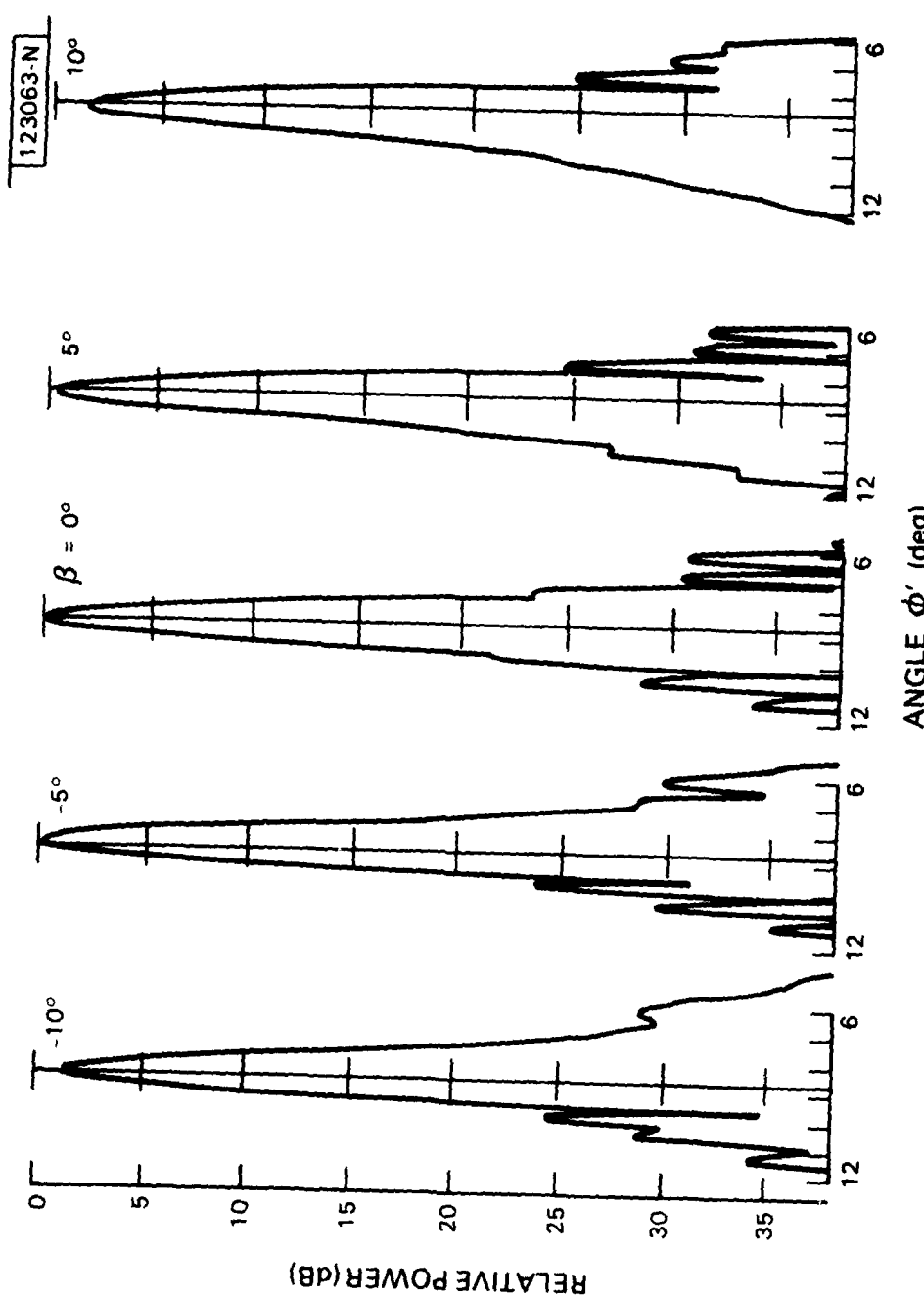
Fig. 19. Measured radiation patterns in scan plane as a function of feed horn tilt angle, β (44.5 GHz; α = 8.6°; φ = 90°).

46
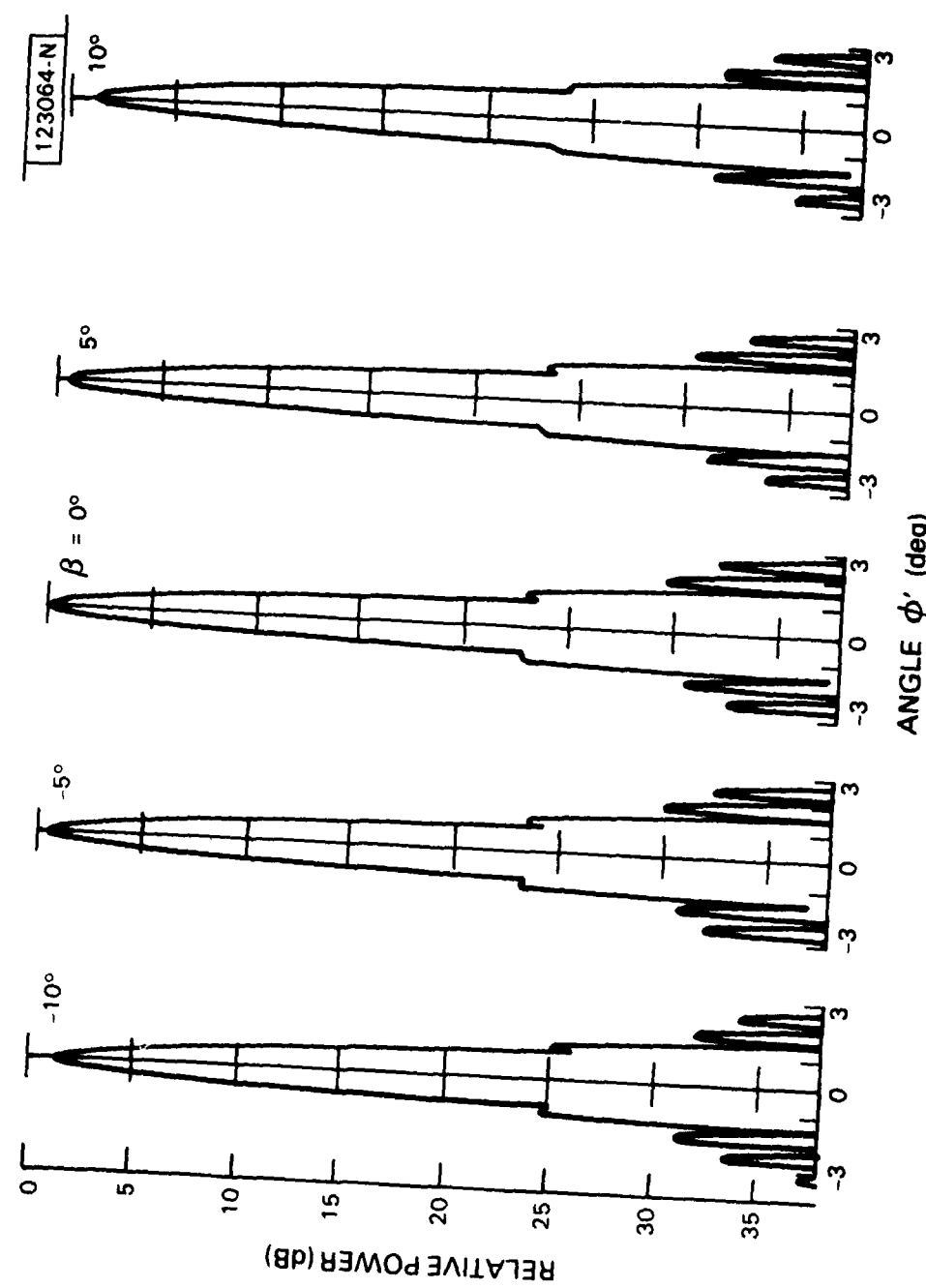
Fig. 20. Measured radiation patterns in orthogonal plane as a function of feed horn tilt angle, β (44.5 GHz; α = 8.6°; φ' = 0).

47

the asymmetrical beam broadening is caused by the differences in edge illumination intensity and scattering at the opposite sides of the lens. The results indicate that the effect of feed horn tilting must be taken into account in multi-beam or scanning lens antenna systems.

VI. EFFECTS OF BEAM SCANNING ON ANTENNA GAIN

The variation in gain of the lens antenna with scan angle and frequency was previously presented in Figure 2 for a specific set of lens parameters where the feed was located on the compromise focal surface. An analysis will now be presented for the general case, from which Figure 2 is obtained, where the feed can be located at any point in the focal region and frequency effects are taken into account. The aperture illumination function $E_m(r)$ is assumed to be rotationally symmetrical and independent of feed position.

The scanning loss $L(\alpha)$ of the antenna, relative to that of an ideal aberrationless lens with the same aperture illumination, can be derived from (Eq. 29) as:

$$L(\alpha) = 20\left[\log\left\{\left|\int_{-\pi/2}^{\pi/2}\int_{0}^{a} E(r,\phi)\, r dr d\phi\right|\right\}\right.$$

$$\left. -\log\left\{\pi \int_{0}^{a} E\left(r_m\right)\, r dr\right\}\right. \qquad\qquad (dB) \qquad\qquad\qquad (31)$$

where

$$E(r,\phi) = E_m(r)\, e^{j\beta(r,\phi)}\;.$$

49

The phase error term $\beta(r,\phi)$ is related to the path length error δ_T by

$$\beta(r,\phi) = 2\pi \ \delta_T/\lambda \tag{32}$$

The total path length error δ_T will now be approximated (using the thin lens theory) as the sum of angle-independent components δ_f and δ_s and an angle-dependent component δ_a:

$$\delta_T = (\delta_f + \delta_s) + \delta_a = (\delta_{fo} + \delta_{so}) \ \hat{r}^2 + \delta_{ao} \ \hat{r}^2 \cos 2\phi \tag{33}$$

Here, δ_{fo}, δ_{so}, and δ_{ao} are the corresponding maximum path length errors at the edge of the lens where (repeating previous Eqs. 10, 11, and 24 for convenience)

$$\delta_{fo} = (\lambda_o - \lambda)N \tag{24}$$

$$\delta_{so} \triangleq (\delta_s)_{max} = \frac{1}{8} \frac{D^2}{f}[\frac{f}{\ell}(1 - \frac{1}{2} \sin^2 \alpha) - 1] \tag{10}$$

$$\delta_{ao} \triangleq (\delta_a)_{max} = \frac{1}{16} \frac{D^2}{f}[\frac{f}{\ell} \sin^2 \alpha] \tag{11}$$

where $D = 2a = $ lens diameter.

δ_{fo} is the frequency-dependent component and δ_{so} and δ_{ao} are the primary spherical and astigmatic components for the path length error δ_T. (N is the total number of steps in the lens.)

The first integral in Eq. 31 can then be written

$$\int_{-\pi/2}^{\pi/2} \int_{0}^{a} E(r, \phi) \, r dr d\phi$$

$$= \int_{-\pi/2}^{\pi/2} \int_{0}^{a} E_m(r) \exp(2\pi j \, \delta_T/\lambda) \, r dr d\phi$$

$$= (a^2) \int_{0}^{\pi} \int_{0}^{1} \{E_m(\widehat{r}) \exp(2\pi j \hat{\delta}_{10} \widehat{r}^2) \exp(2\pi j \, \hat{\delta}_{ao} \, \widehat{r}^2 \cos 2\phi) \widehat{r} d\widehat{r} d\phi\}$$

$$= (\pi a^2)[\int_{0}^{1} E_m(\widehat{r}) \exp(2\pi j \hat{\delta}_{10} x) \, J_o(2\pi \hat{\delta}_{ao} x) dx] \qquad (34)$$

where $\widehat{r} = r/a$, $x = \widehat{r}^2$, $\hat{\delta} = \delta/\lambda$ and $\delta_{1o} = \delta_{fo} + \delta_{so}$.

The decrease in antenna gain is then

$$L(\alpha) = 10 \log_{10}[A] - 20 \log_{10}\{\int_{0}^{1} E_m(\widehat{r}) \, \widehat{r} d\widehat{r}\} \qquad \text{(dB)} \qquad (35)$$

where

$$A = \{[\int_{0}^{1} E_m(\widehat{r}) \cos(2\pi \hat{\delta}_{1o} x) \, J_o(2\pi \hat{\delta}_{ao} x) dx]^2$$

$$+ [\int_{0}^{1} E_m(\widehat{r}) \sin(2\pi \hat{\delta}_{1o} x) \, J_o(2\pi \hat{\delta}_{ao} x) dx]^2\} . \qquad (36)$$

51

Equation 35 may be evaluated numerically for specified value of $E_m(\tilde{r})$, $\hat{\delta}_{1o}$ and $\hat{\delta}_{ao}$. Parametric curves of $L(\alpha)$ versus $\hat{\delta}_{1o}$ with $\hat{\delta}_{ao}$ as an independent parameter and with $E_m(\hat{r}) = 1 - \frac{2}{3}\tilde{r}^2$ are presented in Figure 21 as a set of universal curves to aid in this evaluation. (Note that Figure 2 is the special case of these computations for the compromise locus where $\delta_{so} = 0$). The chosen illumination function $E_m(r)$ provides a taper of 10 dB at the edge of the lens, which is approximately the same level as that provided by the short horn.
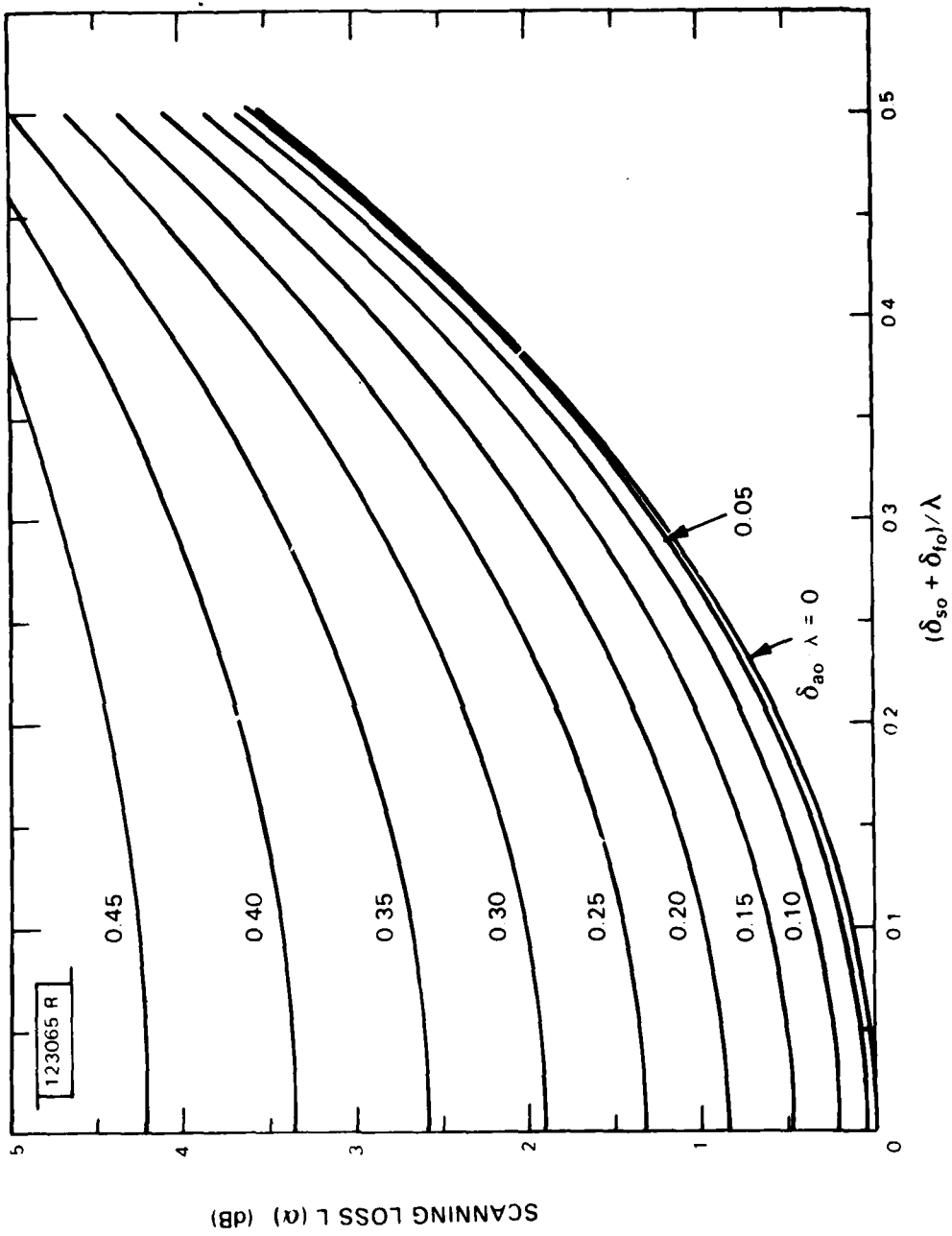
Fig. 21. Scanning loss $L(\alpha)$ versus path length error in zoned lens.

53

VII.   COMPARISON OF MEASURED VERSUS THEORETICAL ANTENNA GAIN

A comparison of the measured and theoretical gain of the lens antenna is complicated by the fact the the E and H plane patterns of the short feed horn are not identical and change with frequency. However, the gain varies with feed position essentially in accordance with theory. As before, only the measurements at 44.5 and 45.5 GHz will be presented because of the strong asymmetry in the 43.5 GHz feed patterns.

The on-axis measured gain and theoretical directivity of the lens with the short horn are compared in Table II for the feed at the focal point. The directivity was computed from both the ray-trace analysis (Method A) and the thin lens approximation, using the gain curves of Figure 21. Also shown for comparison is the directivity for an unzoned lens with the same 10 dB illumination taper (Table II of Reference 13: $m = 1$; $b = 1/2$; $G/G_o = 0.92$), computed from the relation

$$G = 4\pi^2 \left(\frac{a}{\lambda}\right)^2 (G/G_o) \quad . \tag{37}$$

The relative decrease in gain $L(\alpha)$ due to the frequency sensitivity of the lens, which is the difference between corresponding values for the zoned and unzoned lenses, is about 0.2 dB at the band extremities (43.5 and 45.5 GHz). Both the thin lens approximation and Method A give almost identical results for this case. The measured gains at 44.5 GHz and 45.5 GHz are 1.4 and 1.7 dB, respectively, lower than the theoretical directivities. Some of this difference is due to spillover loss from the feed horn, which is

54

TABLE II

On-Axis Gain of Zoned Lens (dBi)

Frequency (GHz)	Method A	Thin Lens Approx.	Unzoned Lens	Measured
43.5	48.0	48.1	48.3	___
44.5	48.6	48.5	48.5	47.2
45.5	48.5	48.5	48.7	46.8

calculated from the averaged E and H plane feed patterns of Figure 14 as 0.7 dB at 44.5 GHz and 0.4 dB at 45.5 GHz. The remaining losses can be attributed to surface reflections and attenuation in the lens, scattering by the zone steps and differences between theoretical and actual primary feed illumination.

The measured gain of the lens decreased by 0.4 dB at 44.5 GHz and 0.2 dB at 45.5 GHz when the feed horn was scanned from its on-axis (α = 0°; ℓ = 35.25") to the maximum off-axis (α = 8.7°; ℓ = 34.85") position on the compromise locus. This agrees reasonably well with the thin lens calculations which predict an additional decrease with scan angle of 0.2 dB from the on-axis values at both frequencies. (The differences between theory and measurement may be due to asymmetrical off-axis feed illumination.)

As a final example, the scanning loss $L(\alpha)$ is plotted in Figure 22 for both 44.5 and 45.5 GHz as a function of distance, ℓ, from the feed to the apex of the lens at the maximum scan angle of 8.7°. The measured values on these graphs exhibit the same general trends as the predictions of the thin lens theory, in that the maximum gain is obtained near the compromise feed locus (ℓ = 34.85") at the 44.5 GHz design frequency and about one inch ($\ell \cong 35.8$") beyond this point at 45.5 GHz. This shift in focal position with frequency represents a cancellation of the frequency-dependent term δ_{fo} with that due to primary spherical aberration δ_{s0}.
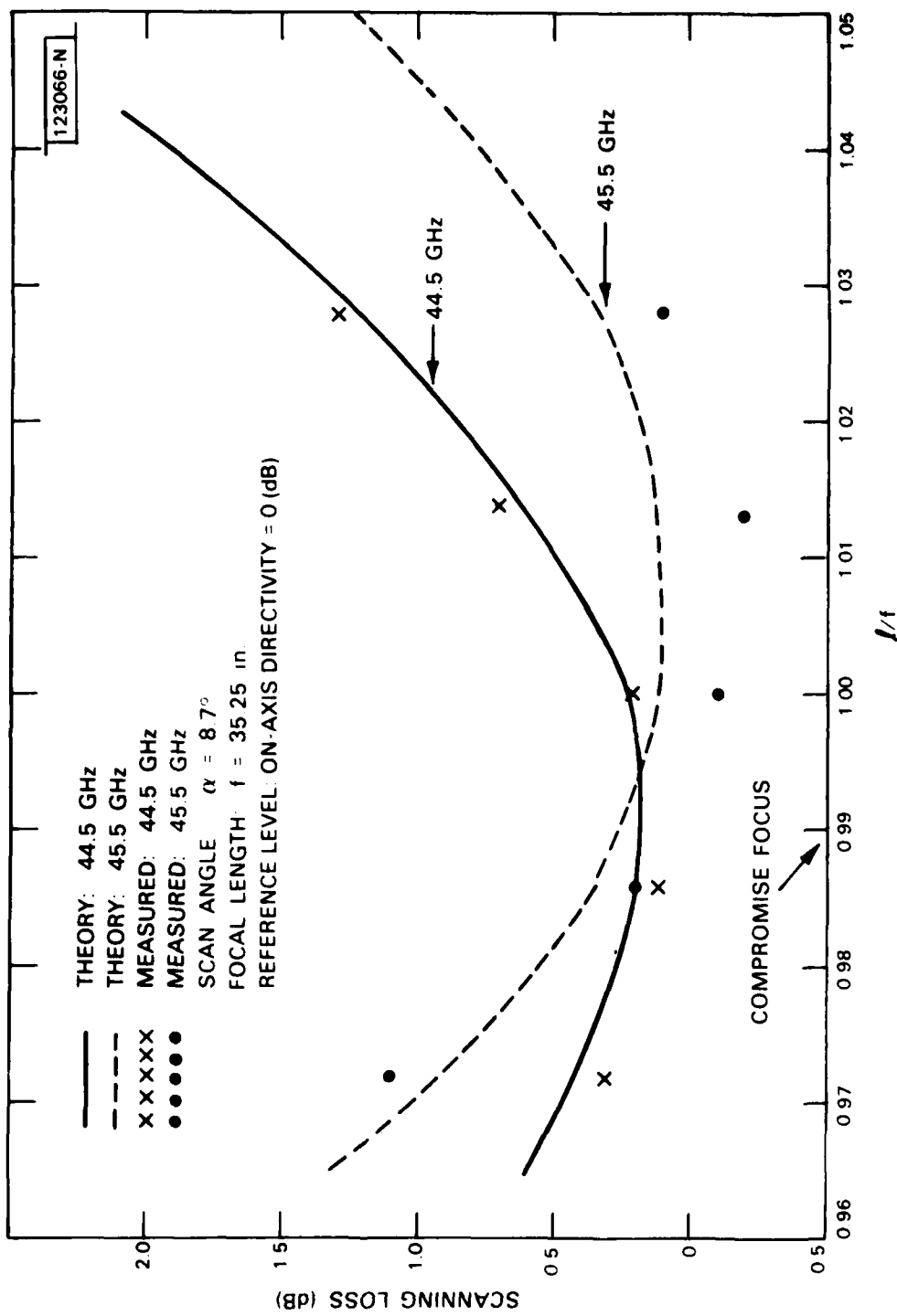
Fig. 22. Scanning loss L(α) of lens antenna with feed position ℓ.

57

VIII. CONCLUSIONS

These measurements and calculations for the 90λ zoned dielectric lens with a fractional degree beamwidth indicate that its electrical performance may be predicted to a high degree of accuracy through the use of geometric optics together with aperture diffraction theory. The most useful approach for preliminary design work is the thin lens approximation, for which the phase aberrations over the lens aperture may be simply computed and their resultant effects upon the antenna gain and radiation characteristics readily ascertained. The geometric ray trace procedures (Methods A and B in this report) could then be used to evaluate the detailed structure of the radiation patterns. In its present form the thin lens analysis assumes a postulated aperture amplitude distribution of radial symmetry. However, this restriction may be readily removed to permit the evaluation of physically realizable primary feeds, including the asymmetries introduced by their movement to off-axis focal positions and by pointing their beams away from the apex of the lens. These off-axis asymmetries in the lens illumination function can occur when a large number of feeds are clustered closely together on the compromise focal surface (or, alternatively, for a single feed which is mechanically scanned by moving a mirror), for which the center of curvature is approximately at the mid-point between the on-axis focus and apex of the lens.

Another problem arises through the restricted space available for the apertures of the multiple feeds on the focal surface of the lens, which leads to difficulties in obtaining proper cross-over levels of the individual beams. However, a preliminary study within our laboratory indicates that the

58

use of conical horn antennas loaded with cylindrical dielectric rods or similar end-fire radiators may resolve this problem while simultaneously reducing the coupling between the feeds.

It should be stressed that the ideally thin lens with a spherical surface which is centered at the focal point is not the only solution for wide-angle scanning optical systems. Friedlander[14], in deriving the differential equations for a generalized dielectric lens which satisfies the Abbé sine criterion, points out that, for a certain range of values of its refractive index, μ), a plano-convex lens nearly satisfies the sine condition and can be considered aplanatic for all practical purposes. In particular, the sine condition is fulfilled both on axis and at the edges of the lens for μ equal to 1.618 and, if the F/D ratio is not too small, will hold to a high degree of accuracy over the whole lens. It is sufficient for μ to be near this value for satisfactory performance. As an example, for $\mu = 1.597$ (polystyrene) and an aperture width equal to the focal length, f, the deviation from the sine condition never exceeds 0.0032f. Friedlander claims that, for an experimental plano-convex lens with this refractive index and a radiating aperture of width 50λ, satisfactory radiation patterns were obtained up to $\pm 10°$ of scan by moving the source at right angles to the axis away from the focus. (He does not make clear whether the lens had a spherical or hyberboloidal front surface, which is required for perfect on-axis collimation.) This design is a simple alternative to the contoured lenses used for moderate aperture applications.

Lee[16] has recently applied computer techniques to determine the shaped contours of a coma-free lens. His measured radiation patterns for a lens with F/D ratio of 1.3 show virtually no coma distortion for a beam scan up to three beamwidths, in contrast to the results for a dielectric lens shaped for a Taylor-type amplitude distribution, instead of the Abbe sine condition, which exhibited pronounced coma distortions. He also applied classical zoning techniques to reduce the weight of the lens and showed how a near-field focus could be obtained by minor modifications of the basic design. The variety of design techniques which are available assure that coma-free dielectric lenses can be tailored at millimeter waves to a wide variety of radar and communication problems.

APPENDIX A

DESIGN PARAMETERS FOR THE 23.5"D ZONED LENS

All equations for the lens design are taken directly from Reference 8. The input parameters to the computer program LENS include the following:

Design wavelength: $\lambda_0 = 0.265$ in.

Radius of front lens surface: $R = 35.25$ in.

Minimum lens thickness: $T_0 = 0.25$ in.

Index of refraction: $\mu = 1.594$ (Rexolite Dielectric)

Subtended Half-Angle of lens at focal point: $\Psi_0 = 19.47°$ (F/D = 1.5)

The output from the computer program includes a sketch of the lens contour (Fig. A-1), a table of points of discontinuity and corners on the lens and a tabular listing of the y-z coordinates of the inner surface. These tabular values may be approximated (to within ± 0.002 inches) by a fourth degree polynomial in y^2 for the central and second zones (zones 1 and 2) and by straight line segments for the remaining five zones, i. e.:

Zone #1: for $5.475 > y > 0$;

$$z = 0.9761 - 1.0226 \times 10^{-2}y^2 + 1.1702 \times 10^{-5} y^4 - 1.4098 \times 10^{-8} y^6 .$$

61

123067-R
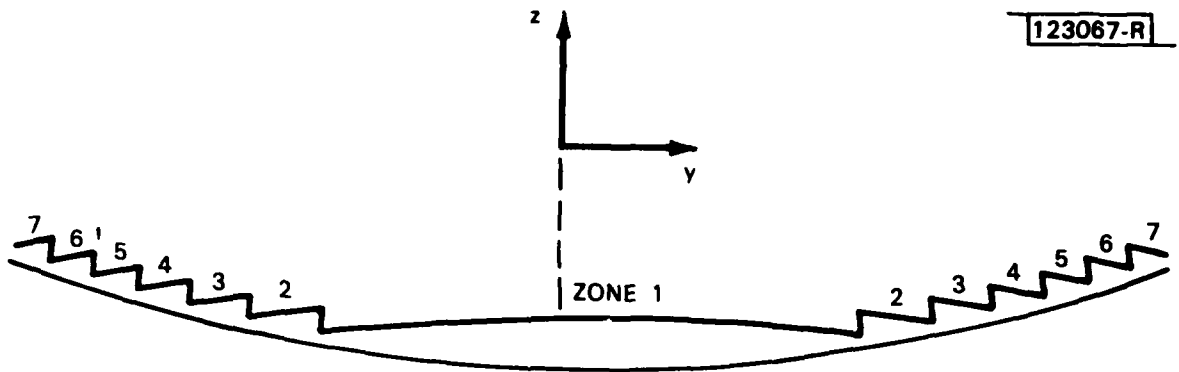
ZONE DIMENSIONS

ZONE	INNER EDGE		OUTER EDGE	
	z	y	z	y
7	2.437	10.846	2.264	11.717
6	2.175	10.014	1.999	10.944
5	1.912	9.098	1.736	10.104
4	1.649	8.071	1.472	9.180
3	1.387	6.882	1.208	8.143
2	1.124	5.427	0.944	6.943
1	0.976	0.0	0.680	5.475

ALL DIMENSIONS IN INCHES

Fig. A-1. Zoned dielectric lens dimensions.

62

Zone #2: for $6.943 > y > 5.427$;

$$z = 1.4368 - 1.1949 \times 10^{-2} \, y^2 + 3.7916 \times 10^{-5} \, y^4 - 2.1473 \times 10^{-7} \, y^6.$$

The origin for the y-z coordinate system is at the apex (front surface/center line) of the lens and all dimensions are in inches. The volume of this lens is 228 cubic inches and its weight 8.6 pounds.

APPENDIX B

RAY TRACE EQUATIONS FOR ZONED LENSES

(Method A)

The procedures and equations used to trace rays in order to determine path length errors in the lens are generally taken (with some modifications) from Chapter IV of Reference 15 and incorporated into the computer program RAYTRACE. This program traces the rays in three dimensions from an arbitrary feed position in the focal region, through the lens and to an aperture plane which is normal to the beam direction α. The feed is assumed, without loss of generality, to lie in the y-z plane at a specified position $P_1(0, y_1, z_1)$, where the coordinate system (x, y, z) has its origin at the apex of the lens (Figure B-1). The ray intersects the rear surface of the lens at the point $P_2(x_2, y_2, z_2)$ or, in cylindrical coordinates, $P_2(r, \phi, z_2)$. (Note that z is negative for the lens surfaces and feed positions.)

The front surface of the lens is a portion of a sphere of radius R, centered at the focal point, which is defined by the equation:

$$\left[x_3^2 + y_3^2 + (R + z_3)^2\right] = R^2 \qquad (B-1)$$

After the ray passes through the lens, it emerges from the front lens surface at the point $P_3(x_3, y_3, z_3)$. The length $\overrightarrow{P_3Q}$ is measured as the perpendicular distance from the front surface of the lens to the reference wavefront plane, which is inclined at an angle α to the x-y plane.

65

Equations (B-2) through (B-10) may be derived from the geometry of Figure B-1 and Snell's Law. The equations of the incident ray segment P_1P_2 from the feed to the rear surface of the lens are given by

$$\frac{x_1 - x_2}{L} = \frac{y_1 - y_2}{M} = \frac{z_1 - z_2}{N} \tag{B-2}$$

where L, M, N are directional cosines:

$$L = \frac{x_2 - x_1}{\ell_1}, \quad M = \frac{y_2 - y_1}{\ell_1}, \quad N = \frac{z_2 - z_1}{\ell_1} \tag{B-3}$$

and $\ell_1{}^2 = |\overrightarrow{P_1P_2}|^2 = (x_2 - x_1)^2 + (y_2 - y_1)^2 + (z_2 - z_1)^2$.

Each zone of the rear lens surface is represented by a polynomial in r^2 in the parametric form of Eq. B-4 (note change from y^2 in Appendix A to r^2):

$$F_n(r,z_2) = \frac{1}{2} c_{1n} r^2 + b_{4n} r^4 + b_{6n}r^6 + b_{8n}r^8 - (z_2 + g_n) = 0,$$
$$n=1,2,3,\ldots N$$

(Eq. 4.33 of Ref. 15)

$$\tag{B-4}$$

where n is the zone number, corresponding to the given value of r.

The tangent plane at the point P_2 on the rear lens surface is defined by the angles:

$$(\alpha_r, \beta_r, \gamma_r) = \frac{(\frac{\partial F}{\partial x}, \frac{\partial F}{\partial y}, \frac{\partial F}{\partial z})}{\{(\frac{\partial F}{\partial x})^2 + (\frac{\partial F}{\partial y})^2 + (\frac{\partial F}{\partial z})^2\}^{1/2}} \tag{B-5}$$

(Eq. 4.24 of Ref. 15)

66

Fig. B-1. Ray path in lens antenna ($\overrightarrow{P_1 P_2 P_3 \hat{r}}$).

123068-N

COORDINATES

P_1 (O, Y_1, Z_1) — FEED
P_2 (X_2, Y_2, Z_2) — REAR LENS SURFACE
P_3 (X_3, Y_3, Z_3) — FRONT LENS SURFACE
P_0 (X_0, Y_0, O) — TRANSFER PLANE

$\Delta = \overrightarrow{P_3 P_0}$

67

where

$$\frac{\partial F}{\partial X} = (c_{1n} + 4\, b_{4n}r^2 + 6\, b_{6n}r^4 + 8\, b_{8n}r^6)x_2 = H_n\, x_2 \triangleq F_x$$

$$\frac{\partial F}{\partial y} \triangleq F_y = H_n\, y_2$$

$$\frac{\partial F}{\partial y} \triangleq F_z = -1$$

Also:

$$F_T = \left(F_x^{\,2} + F_y^{\,2} + 1\right)^{1/2}$$

Then:

$$\alpha_r = F_x/F_T, \quad \beta_r = F_y/F_T, \quad \gamma_r = -\,1/F_T \qquad\qquad (B\text{-}6)$$

The angle, I, between the ray segment $\overline{P_1P_2}$ and the normal to the tangent plane at P_2 is given by:

$$\cos I = \alpha_r L + \beta_r M + \gamma_r N \qquad (\text{Eq. 4.17 of ref. 15}) \qquad (B\text{-}7)$$

The angle of refraction I'_n at P_2 is determined from Snell's law:

$$\mu \cos I' = \left\{\mu^2 - (1 - \cos^2 I)\right\}^{1/2} \qquad (\text{Eq. 4.17 of ref. 15}) \qquad (B\text{-}8)$$

The directional cosines L', M', N' of the ray segment $\overline{P_2P_3}$ at point P_2 are given by:

$$\mu L' - L = \kappa \, \alpha_r \qquad\qquad \text{(Eq. 4.2 of Ref. 15)} \qquad \text{(B-9)}$$

$$\mu M' - M = \kappa \, \beta_r$$

$$\mu N' - N = \kappa \, \alpha_r$$

where $\kappa = \mu \cos I' - \cos I$. $\qquad\qquad$ (Eq. 4.3 of Ref. 15). $\qquad$ (B-10)

The intersection coordinates $P_3(x_3, y_3, z_3)$ of ray segment $\overline{P_2 P_3}$ at the front lens surface are determined by first calculating the intercept point P_0 (x_0, y_0) of this ray with a transfer plane which is perpendicular to the axis of symmetry (z axis) and passes through the apex of the lens; the ray is then backtracked along $\overline{P_2 P_0}$ from P_0 to P_3 on the spherical lens surface. (See Section 4.3 of Reference 15 for details). The coordinates x_0, y_0 are given by:

$$x_o = x_2 - \frac{L'}{N'}(z_2) \qquad\qquad \text{(Eq. 4.4 of Ref. 15)} \qquad \text{(B-11)}$$

$$y_o = y_2 - \frac{M'}{N'}(z_2)$$

We next calculate

$$V = -\frac{1}{R}\left(x_o^2 + y_o^2\right) \qquad\qquad \text{(Eq. 4.9 of Ref. 15)} \qquad \text{(B-12)}$$

$$U = N' + \frac{1}{R}\left(L' \, x_o + M' \, y_o\right) \qquad\qquad \text{(Eq. 4.10 of Ref. 15)} \qquad \text{(B-13)}$$

and

$$\Delta = \frac{V}{U + \sqrt{U^2 + V/R}}$$ (Eq. 4.12 of Ref. 15)   (B-14)

(Δ is the negative value of line segment $P_0 P_3$.)

Then:

$$x_3 = L'\Delta + x_o$$ (Eq. 4.5 of Ref. 15)   (B-15)

$$y_3 = M'\Delta + y_o$$

$$z_3 = N'\Delta$$

We have now calculated the coordinates of P_1, P_2, and P_3. The lengths of ray segments $\overrightarrow{P_1 P_2}$, $\overrightarrow{P_2 P_3}$, and $\overrightarrow{P_3 Q}$ can then be obtained from the relations:

$$\alpha_s = \tan^{-1}(y_1/z_1)$$ (B-16)

$$\gamma_s = \tan^{-1}(z_3/y_3)$$ (B-17)

$$\xi_s = \gamma_s + \alpha_s$$ (B-18)

Also

$$y_2 = r \sin \phi$$ (B-19)

$$x_2 = r \cos \phi$$ (B-20)

70

The optical path length ℓ_T of the ray is obtained from the relation:

$$\ell_T = \ell_1 + \mu\ell_2 + \ell_3 \quad . \tag{B-21}$$

$$\ell_1 = |\overrightarrow{P_1 P_2}| = \{(x_1 - x_2)^2 + (y_1 - y_2)^2 + (z_1 - z_2)^2\}^{1/2} \tag{B-22}$$

$$\ell_2 = |P_1 P_3| = \{(x_2 - x_3)^2 + (y_2 - y_3)^2 + (z_2 - z_3)^2\}^{1/2} \tag{B-23}$$

$$\ell_3 = |P_3 Q| = -\{y_3^2 + z_3^2\}^{1/2} \sin \xi_s \tag{B-24}$$

The path length error $\Delta\ell_T(r,\phi)$ is defined as the difference between the length, ℓ_T, of this general ray and that of the principal ray, ℓ_{TP}, which is chosen as that ray which intercepts the rear lens surface at $(0, 0, -g_N)$. Then:

$$\Delta\ell_T(r,\phi) \quad \ell_T - \ell_{TP} \tag{B-25}$$

where

$$\ell_{TP} \triangleq \ell_T \big|_{r=0} \tag{B-26}$$

Figure 9 of the text shows this path length error, $\Delta\ell_T(r,\phi)$ [mod λ], versus the radial lens distance, r, for two feed positions ($\alpha = 0°$ and $8.6°$) on the compromise focal arc and for ϕ equal to $0°$, $45°$, and $90°$. These plots

71

were obtained from the computer program RAYTRACE which incorporated the equations listed in this Appendix. The RAYTRACE program was also used for the phase constant, $\beta(r,\phi)$, as input to the programs for calculating radiation patterns and gain of the lens antennas (Appendix C) where

$$\beta(r,\phi) = 2\pi \, \Delta \ell_T(r,\phi)/\lambda \quad . \tag{B-27}$$

APPENDIX C

CALCULATION OF GAIN AND RADIATION PATTERNS OF ZONED LENS

(Method A)

A computer program was generated for calculating the directive gain and radiation patterns of the lens antenna, based upon Eqs. 29 and 32 of the text. This section presents details of these calculations:

Equation 32 for the antenna gain G (α) is repeated here for convenience:

$$G(\alpha) = [8/\lambda^2]\left\{\frac{\left|\int_{-\pi/2}^{\pi/2}\int_0^a E(r,\phi)\ r\ dr\ d\phi\right|^2}{\int_0^a |E(r,\phi)|^2\ r\ dr}\right\} \qquad (32)$$

This equation represents an integration of the near fields over the lens aperture. However, we will take the integration over the projection of the lens aperture upon that wavefront aperture plane which is perpendicular to the beam direction. Although this projected area is elliptical rather than circular in cross-section, this distortion will be slight if the beam tilt angle is small so that the projected area can be assumed to be of the same size as the lens aperture. Additionally, the obliquity factor is assumed to be negligible in the radiation integral, and a thin lens approximation is made in which the cylindrical coordinates (r,ϕ) of the ray at the rear lens surface are approximated by those (r,ϕ) in the tilted coordinate system (X',Y',Z') of the projected aperture plane (Figure B-1). Under these conditions, Eq. 29 will still be applicable.

The denominator of Equation 29 may be evaluated in closed form when $E(r, \phi)$ is the analytical expression given by Equation 30:

$$|E(r,\phi)| \triangleq E_m(\hat{r}) = E_0\left(1 - \frac{2}{3}\hat{r}^2\right) \tag{30}$$

where

$$\hat{r} = 2r/D = r/r_N$$

Then:

$$\int_0^a |E(r,\phi)|^2 dr = E_0^2 \int_0^1 \left(1 - \frac{2}{3}\hat{r}^2\right)\hat{r} \ d\hat{r} = \frac{13}{54} \ . \tag{C-1}$$

Approximating the double integral of Equation 32 by a double summation over ϕ and r and utilizing Eq. (C-1), we have:

$$G(\alpha) = 8K\left(\frac{r_N}{\lambda}\right)^2 \left(\frac{1}{E_0}\right)^2 \left|\sum_\phi \sum_r E(\hat{r}) \ \hat{r} \ \Delta\hat{r} \ \Delta\phi\right|^2 \tag{C-2}$$

where $K = 54/13$ for the 10 dB tapered illumination of Equation 30. (Similarly, $K = 2$ for uniform illumination.)

We will perform the double summation by dividing the central zone of the lens into equally-sized incremental areas and then adding the contributions from the outer zones. The summation over ϕ can be carried out over a semi-circle due to symmetry. Dividing the semi-circle from $\pi/2 > \phi > -\pi/2$ into q angular sectors, each of which is centered at ϕ_i:

$$\phi_i = \frac{\pi}{2}\left[1 - \frac{1}{q}(2i - 1)\right] \qquad (C-3)$$

where $\Delta\phi = \pi/q$ $\quad i = 1,2,3,\ldots,q$

Similarly, the central zone is divided into radial annuli of equal area for which each mean radius $\hat{r}_k$ is located at

$$\hat{r}_K = \frac{1}{2}\left[\left(\frac{k}{p}\right)^{1/2} + \left(\frac{k-1}{p}\right)^{1/2}\right]\hat{r}_c \qquad (C-4)$$

and

$$\Delta\hat{r}_K = \left[\left(\frac{k}{p}\right)^{1/2} - \left(\frac{k-1}{p}\right)^{1/2}\right]\hat{r}_c \qquad k=1,2,3,\ldots,p$$

$$\hat{r}_c = r_c/r_N$$

r_N = outer radius of lens

r_c = radius of central zone.

For the outer zones, the radial width of each annulus is arbitrarily made equal to the width of the zone. Equation C-2 for the antenna gain $G(\alpha)$ can then be written (omitting several algebraic steps):

$$G(\alpha) = A\left\{\left[\left(\frac{\hat{r}_c^{\,2}}{p}\right) \cdot B + C\right]^2 + \left[\left(\frac{\hat{r}_c^{\,2}}{p}\right) \cdot D + F\right]^2\right\} \qquad (C-5)$$

where

$$A = \left(\frac{2\pi^2 K}{q^2}\right)\left(\frac{r_N}{\lambda}\right)^2$$

The factors B, C, D, and F represent the contributions from the various zones. The contributions from the central zone are given by the quadrature components B and D:

$$B = \sum_{i=1}^{q} \sum_{k=1}^{p} E_M(\hat{r}_k) \cos \beta(\hat{r}_k, \phi_i)$$

$$D = \sum_{i=1}^{q} \sum_{k=1}^{p} E_M(\hat{r}_k) \sin \beta (\hat{r}_k, \phi_i) \tag{C-6}$$

The phase constant

$$\beta(\hat{r}_k, \phi_i) = 2\pi \Delta \ell_T / \lambda \left| \begin{array}{l} \hat{r} = \hat{r}_k \\ \phi = \phi_i \end{array} \right. \tag{C-7}$$

is obtained from the ray trace program of Appendix B.

Similarly, the contributions from the outer zones are given by the factors C and F:

$$C = \sum_{i=1}^{q} \sum_{n=2}^{N} E_M(\hat{r}_{on}) \cdot (\hat{r}_n^2 - \hat{r}_{n-1}^2) \cdot \cos \beta(\hat{r}_{on}, \phi_i)$$

$$F = \sum_{i=1}^{q} \sum_{n=2}^{N} E_M(\hat{r}_{on}) \cdot (\hat{r}_n^2 - \hat{r}_{n-1}^2) \cdot \sin \beta(\hat{r}_{on}, \phi_i) \tag{C-9}$$

where

$$\hat{r}_{on} = 1/2(\hat{r}_n + \hat{r}_{n-1})$$

r_n is the outer radius of nth zone ($n=1$ for central zone).

An obvious modification of Eq. (C-5) for greater accuracy in evaluating $G(\alpha)$ is to use a finer grid for the contributions from the outer zones. However, the results obtained for the experimental lens agreed within about 0.1 dB with those obtained from other programs, so this was not judged to be necessary.

The far-field amplitude $F(\theta',\phi')$ is calculated from Eq. 26, which is an integral of similar form to that for $G(\alpha)$, except that the phase constant $\beta(r,\phi)$ must be replaced by $\beta(r,\phi,\theta',\phi')$ where θ' and ϕ' are the polar coordinates for the radiated field and

$$\hat{\beta}(\hat{r}_k,\phi_i,\theta',\phi') =$$

$$\beta(\hat{r}_k,\phi_i) + (\frac{2\pi r_N}{\lambda}) \left[\hat{r}_k \sin \theta' \cos(\phi' - \phi_i) \right] \quad .$$

The techniques for replacing the double integrals by double summations then follow the previous procedures.

REFERENCES

1. W. C. Cummings, P. C. Jain, and L. J. Ricardi, "Fundamental Performance Characteristics that Influence EHF MILSATCOM Systems," IEEE Trans. Commun. COM-27, 1423 (1979), DDC-AD-A084591/7.

2. L. J. Ricardi, "Communication Satellite Antennas," Proc. IEEE 65, 356 (1977), DDC-AD-A063415/4.

3. J. F. Ramsay, "A Universal Scanning Curve for Wide-Angle Mirrors and Lenses," Marconi Review, XVIII, 150-159 (1956).

4. J. F. Ramsay and J. A. C. Jackson, "Wide-Angle Scanning Performance of Mirror Aerials," Marconi Review, XIX, pp. 119-140 (1956).

5. E. A. Ohm, "A Proposed Multiple-Beam Microwave Antenna for Earth Stations and Satellites," Bell Sys. Tech. J., 53, 1657-1665 (1974). (Also reprinted in Electromagnetic Horn Antennas, A. W. Love, Ed. (IEEE Press, New York, 1976) p. 281.

6. H. Jasik, Antenna Engineering Handbook, (McGraw-Hill, New York 1961), p. 14-6.

7. T. C. Cheston and D. H. Shinn, "Scanning Aberrations of Radio Lenses," Marconi Review, XV, 174-184 (1952).

8. D. H. Shinn, "The Design of a Zoned Dielectric Lens for Wide Angle Scanning," Marconi Review, XVIII, 37-47 (1955).

9. M. Born and E. Wolf, Principles of Optics, (Pergamon Press, New York, 1964), p. 211.

10. R. H. Clarke and J. Brown, "Diffraction Theory and Antennas," Section 7.2.3, Eq. 7.48, (Halsted Press [Division of Wiley & Sons], 1980), p. 196.

11. P. D. Potter, "A New Horn Antenna With Suppressed Sidelobes and Equal Beamwidths," Microwave, XI, 71-78 (1963). (Also reprinted in Electromagnetic Horn Antennas, A. W. Love, Ed. (IEEE Press, New York 1976), p. 201.)

12. R. H. Turrin, "Dual Mode Small-Aperture Antennas," IEEE Trans. Antennas Propag. AP-15, 307 (1967). (Also reprinted in Electromagnetic Horn Antennas, A. W. Love, Ed. (IEEE Press, New York, 1976), p. 214.)

13. M. I. Skolnik, Radar Handbook," (McGraw-Hill, New York, 1970) p. 9.

REFERENCES (cont'd)

14. F. G. Friedlander, "A Dielectric-Lens Aerial for Wide-Angle Beam Scanning," Inst. Elec. Eng., 93, Pt. 3A, 658-662 (1946).

15. W. Welford, Aberrations of the Symmetrical Optical System (Academic Press, New York 1974).

16. J. J. Lee, "Numerical Methods Make Lens Antennas Practical," Microwaves 21, 81-84 (1982).

Acknowledgments

SECURITY CLASSIFICATION OF THIS PAGE *(When Data Entered)*

REPORT DOCUMENTATION PAGE		READ INSTRUCTIONS BEFORE COMPLETING FORM
1. REPORT NUMBER ESD-TR-82-102	2. GOVT ACCESSION NO. AD - A126214	3. RECIPIENT'S CATALOG NUMBER
4. TITLE *(and Subtitle)* EHF Dielectric Lens Antenna for Satellite Communication Systems		5. TYPE OF REPORT & PERIOD COVERED Technical Report
		6. PERFORMING ORG. REPORT NUMBER Technical Report 620
7. AUTHOR(s) Walter Rotman		8. CONTRACT OR GRANT NUMBER(s) F19628-80-C-0002
9. PERFORMING ORGANIZATION NAME AND ADDRESS Lincoln Laboratory, M.I.T. P.O. Box 73 Lexington, MA 02173-0073		10. PROGRAM ELEMENT, PROJECT, TASK AREA & WORK UNIT NUMBERS Program Element Nos. 63431F and 33601F Project Nos. 2029 and 6430
11. CONTROLLING OFFICE NAME AND ADDRESS Air Force Systems Command, USAF Andrews AFB Washington, DC 20331		12. REPORT DATE 3 January 1983
		13. NUMBER OF PAGES 90
14. MONITORING AGENCY NAME & ADDRESS *(if different from Controlling Office)* Electronic Systems Division Hanscom AFB, MA 01731		15. SECURITY CLASS. *(of this report)* Unclassified
		15a. DECLASSIFICATION DOWNGRADING SCHEDULE

16. DISTRIBUTION STATEMENT *(of this Report)*

Approved for public release; distribution unlimited.

17. DISTRIBUTION STATEMENT *(of the abstract entered in Block 20, if different from Report)*

18. SUPPLEMENTARY NOTES

None

19. KEY WORDS *(Continue on reverse side if necessary and identify by block number)*

EHF technology	millimeter wave antenna
dielectric lens antenna	multi-beam antenna
satellite communication	

20. ABSTRACT *(Continue on reverse side if necessary and identify by block number)*

Dielectric lens antennas are applicable to the design of multiple-beam antenna (MBA) systems on EHF communication satellites. Advantages include excellent wide angle scanning properties and elimination of feed blockage. This report describes an experimental 90λ dia. zoned dielectric lens, operating at 44 GHz, which was fabricated and tested in order to estimate the performance of a dielectric lens MBA. Measurements showed that the lens generated a beam with a half-power beamwidth (HPBW) of 0.7° which could be steered over a total scan angle of 18° (corresponding to the earth's field-of-view from a geosynchronous satellite) with a scanning loss of less than 1 dB and a gain in excess of 47 dBi measured at the sub-satellite point over a 5% bandwidth. A theoretical analysis of the radiation characteristics of the lens antenna, using ray tracing and geometric optics techniques, gave excellent agreement with the measurements. Simplified design equations were developed to facilitate evaluation and development of lens antenna systems of this type.

DD FORM 1473 EDITION OF 1 NOV 65 IS OBSOLETE
1 Jan 73